Ana Bárbara de Sousa Carreira

Licenciada em Bioquímica

Mechanisms underlying intracellular delivery

Dissertação para obtenção do Grau de Mestre em Biotecnologia

Orientadora: Sara Figueiredo, Postdoctoral Research Fellow, FCT/UNL

Co-orientador: Pedro Viana Baptista, Professor associado com agregação, FCT/UNL

Júri:

Presidente: Professor Doutor Pedro Miguel Calado Simões
Arguente: Doutor Pedro Miguel Martinho Borralho
Vogal: Doutora Sara Rute Carvalhal de Figueiredo

FACULDADE DE CIÊNCIAS E TECNOLOGIA
UNIVERSIDADE NOVA DE LISBOA

Setembro 2015

MECHANISMS UNDERLYING INTRACELLULAR DELIVERY

ACKNOWLEDGEMENTS

This work would not have been possible without the help of people and institutions that contributed to its accomplishment. I would like to specially thank:

Sara Figueiredo, my supervisor, for all the support and guidance, for endless discussions and constant support. For my personal a scientifically growth during this year, for trusting me this project and for believing in me. Thank you, I am grateful for this opportunity.

Professor Pedro V. Baptista, my co-supervisor, for once more giving the opportunity to develop a project in his working group. I would like to thanks for all the support, for my scientific growth he promoted during this project, and above all things for trusting me.

All members of the lab 315, Fábio Carlos, Milton Cordeiro, Raquel Vinhas, Rita Cabral, João Jesus, Ana Sofia, Pedro Pedrosa, Letícia Giestas, Miguel Larguinho, I would like to thank you for the awesome time in the lab, and for all the support and advisors.

Marisa e Rafaela, I would like to thank for friendship and companionship, for the support given in the good and especially in the bad moments. For all of this and much more, thank you!

My friends, for always being there and for all the relaxation moments.

My closest family, I would like to thank you for unconditional support and guidance, for all the patience, and for forgiven for all the time that I had been way.

Luís, for all love and affection, for all support and understanding.

Bárbara Carreira

RESUMO

AuNPs são utilizadas como sistemas versáteis em diversas aplicações na área da biomedicina, incluindo em entrega de fármacos e imagem celular. Estes sistemas são responsáveis pelo transporte de moléculas ativas, um passo considerado como um problema crucial em entrega de fármacos. Assim sendo, de forma a desenvolver AuNPs multifuncionais para aplicações específicas e eficientes, é necessário compreender o mecanismo pelo qual as AuNPs interagem com células vivas.

O principal objetivo deste trabalho consistiu na análise do mecanismo de internalização celular de AuNPs esféricas de 14 nm na linha celular A549, através de espectroscopia e microscopia de fluorescência em combinação com análise quantitativa obtida por ICP-MS. As AuNPs marcadas com TAMRA foram caracterizadas por espectroscopia de UV-visível e fluorescência, sendo obtido por DLS um diâmetro hidrodinâmico final de 22.5 ± 0.33 nm. Relativamente aos estudos de internalização celular, as AuNPs apresentaram uma rápida cinética de internalização celular, alcançando o ponto de saturação após 6 horas de incubação na linha celular A549. Estudos adicionais relacionados com o mecanismo de internalização destas AuNPs foram conduzidos utilizando inibidores específicos para cada via de endocitose. A inibição mais pronunciada foi obtida após utilização de clorpromazina, um inibidor de endocitose mediada por clatrina, resultando na diminuição da internalização de AuNPs em 23.5% após 1 hora de incubação. Este resultado preliminar obtido por espectroscopia de fluorescência indica a internalização destas AuNPs predominantemente por endocitose mediada por clatrina, sugerindo que outras vias de endocitose podem estar envolvidas na internalização celular destas AuNPs. Em termos de viabilidade celular, as AuNPs preparadas e os inibidores de endocitose não revelaram efeitos nefastos significativos na viabilidade celular da linha A549.

Palavras-chave: Inibição de endocitose, nanopartículas de ouro, mecanismos de internalização, nanomedicine

ABSTRACT

AuNPs are versatile systems used for different biomedical application including imaging, drug and gene delivery. These systems support the intracellular transport of active molecules, a step that is considered one of the crucial problems in drug delivery. Nevertheless, in order to design optimal multifunctional AuNPs for specific and efficient nanomedicine applications, the mechanism by which AuNPs interact with living cells must be fully understand.

The main goal of this work consisted in the assessment of the cellular uptake mechanism of 14 nm spherical AuNPs by A549 cells, through fluorescent spectroscopy and microscopy, in combination with quantitative analysis by ICP-MS. TAMRA labeled AuNPs were characterized by UV-visible and fluorescent spectroscopy and the final hydrodynamic diameter of 22.5 ± 0.33 nm was obtained by DLS. Regarding the cellular uptake studies, the AuNPs presented a fast cellular uptake kinetics reaching a saturation point after 6 hours of incubation in A549 cells. Further investigation concerning the internalization mechanism of this AuNPs was evaluated using specific inhibitors for different endocytic pathways. Optimal inhibition was achieved using chlorpromazine, inhibitor of clathrin-mediated endocytosis, resulting in a 23.5 % inhibition of AuNPs after 1 hour of incubation. This preliminary result obtained by fluorescent spectroscopy suggests that these AuNPs were predominantly uptake by clathrin-mediated endocytosis, meaning that other endocytic pathways must be involved in the cellular uptake of this AuNPs. In what cell viability is concern, the prepared AuNPs and the endocytic inhibitors revealed no significant effect on the cell viability in A549 cell line.

Keywords: Endocytic inhibition, gold nanoparticles, internalization mechanisms, nanomedicine

TABLE OF CONTENTS

FIGURES INDEX

TABLES INDEX

ABREVIATIONS

A549	Human lung carcinoma cell line
AFM	Atomic force microscopy
AP	Adaptor protein
AUC	Area under the curve
AuNPs	Gold nanoparticles
CCP	Clathrin coated pits
CCV	Clathrin coated vesicles
CIE	Clathrin-independent endocytosis
CME	Clathrin-mediated endocytosis
CT	Computed tomography
DLS	Dynamic light scattering
DMEM	Dulbecco's modified eagle medium
EPR	Enhanced permeability and retention
FBS	Fetal bovine serum
FDA	Federation of food and administration
FRET	Förster resonance energy transfer
ICP-MS	Inductively coupled plasma mass spectrometry
MRI	Magnetic resonance imaging
NP	Nanoparticle
PEG	Poly(ethylene) glycol
PET	Positron emission tomography
RT	Room temperature
SPR	Surface plasmon resonance
SERS	Surface enhanced Raman spectroscopy
SD	Standard deviation
TEM	Transmission electron microscopy
TAMRA	Tetramethylrhodamine cadaverine

I. INTRODUCTION

1. NANOTECHNOLOGY

Nanotechnology is an interdisciplinary field involving different research areas, namely biology, chemistry, engineering and medicine (Cai et al., 2008). It can be defined as the creation of useful and functional structures, devices and systems by controlling the matter at a nanometer scale (1 - 100 nm) (Daniel and Astruc, 2004). This field is based on the chemical synthesis of controllable size and shape nanoparticles with distinctive optical, electronic and magnetic properties (Chithrani et al., 2006). The development of these new materials with tunable properties prompted the growth of this field, and nanoparticles are nowadays used for a wide range of applications. In particular, the interest in using nanoparticles for biomedical applications, including in therapeutic and diagnostic applications, increased since their size scale is similar to functional components of living cell and biological molecules (ex. DNA and proteins) (Chithrani et al., 2006; Eustis and El-Sayed, 2006). The improvement of biomedical applications by using nanoparticles based systems, such as molecular diagnostics, drug and gene delivery and therapeutics, stimulated the foundation of a new emerge field, nanomedicine (Jain, 2008).

1.1. NANOMEDICINE

Nanomedicine emerged from the application of nanotechnology to medicine (Jain, 2008), taking advantage of nanoscale size systems to improve diagnostics and therapeutics (Sahay et al., 2010). Liposomes (Park et al., 2004), quantum dots (Cai et al., 2006), carbone nanotubes (Liu et al., 2007), silver and gold nanoparticles (Huang et al., 2007) are examples of nanoparticles used in nanomedicine (Figure I.1).

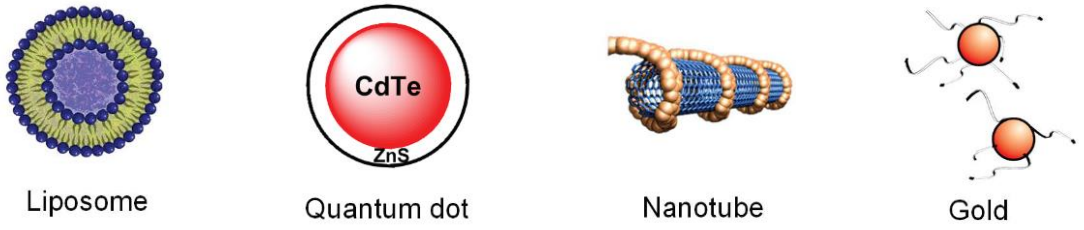

Figure I.1 - Different types of nanoparticles used in nanomedicine. (A) Liposome; (B) Quantum dot; (C) Carbon nanotube; (D) Gold nanoparticles (Adapted from Cai et al., 2008).

These nanomedicines can delivery molecules with low molecular weight more efficiently and selectively to a specific region of interest, improving the clinical benefit and also decreasing the toxicity to healthy tissues (Boisselier and Astruc, 2009; Sahay et al., 2010; Lammers et al., 2011). Besides drug delivery for therapeutic applications, nanomedicines have been exploited for imaging applications aiming at improved diagnostics (Lammers et al., 2011). Furthermore, new systems and strategies are being developed for theranostic applications, in which nanomedicines are used for diagnostic and therapeutic

simultaneously. Due to unique optical and physiochemical properties, gold nanoparticles (AuNPs) are one of the most common type of nanomedicines that has being extensively used for a variety of theranostic purposes, including cancer therapy, *in vivo* imaging and drug delivery. (Boisselier and Astruc, 2009; Cai et al., 2008; Lammers et al., 2011).

1.2. GOLD NANOPARTICLES

Colloidal AuNPs first appeared in antiquity for decoration purposes due to their optical properties, in particular for staining glass. Scientifically, the first comprehensive studies report to Faraday (1857), which attributed the red color of gold nanoparticles to their colloidal nature, observing that colloidal gold had different properties from the bulk. Since then, colloidal gold gained increasing interest due to its remarkable features, providing the development of new devices and systems with countless potential applications in many biological fields, as molecular diagnostic, imaging, drug delivery and therapeutics (Baptista et al., 2008; Sperlinger et al., 2008; Boisselier and Astruc, 2009).

This increasing interest in study gold nanoparticles (AuNPs) is based on their exceptional characteristics, such as unique optical and electronic properties, high stability and biocompatibility, easy surface functionalization, and controllable size and shape in a scale range of 3 - 200 nm, leading to the development of a wide range of AuNPs based systems (Sperlinger et al., 2008; Boisselier and Astruc, 2009; Vigderman and Zubarev, 2013; Conde et al., 2014).

One of the most important characteristics of AuNPs is their surface plasmon resonance (SPR), resulting in great optical properties. The SPR effect is based on the collective oscillation of conduction electrons at the AuNP surface, generated by the interaction of electromagnetic wave in the electrons at the AuNP surface. This effect translates into high absorption coefficients and scattering properties, allowing the utilization of spectroscopic techniques for optical detection methods and biological imaging by microscopy techniques (Jain et al., 2006; Boisselier and Astruc, 2009). Typically, 14 nm spherical AuNPs present a SPR absorption band around at 520 nm. However, this band highly depends on size, shape, inter-particle distance and dielectric properties of environment of AuNPs (Baptista et al., 2008; Jain et al., 2006).

1.2.1. SYNTHESIS

The utilization of AuNPs for different purposes relies on the ability to synthetize nanoparticles with desired and adequate size and shape, and surface modifications (Tiwari et al., 2011). Different methods have been reported for AuNP synthesis. Typically, AuNP preparation is based on chemical reduction of gold (III) to gold (0) in presence of a capping agent. This agent is able to bind to the nanoparticle surface, blocking the growth of nanoparticles and allowing stabilization in solution. The control of AuNPs' morphology is achieved by adjusting reaction conditions, such as time, temperature and capping agent (Baptista et al., 2008)

The most commonly used methods for spherical AuNPs synthesis are based on the citrate reduction method first purposed by Turkevich in 1951 (Turkevich et al., 1951). In this method, citrate is used both as reducer and capping agent, and the AuNP diameter is achieved by carefully controlling the ratio citrate/gold. This method allows the synthesis of AuNPs with diameter within 9 - 120 nm range, where the increase of citrate promotes smaller particles. The citrate also allows the stabilization of AuNPs in solution and permits further functionalization, since it can be easily replaced by molecules with high affinity to gold, such as thiolated biomolecules (Baptista et al., 2008; Tiwari et al., 2011; Vigderman and Zubarev, 2013).

1.2.2. FUNCTIONALIZATION

Functionalization of AuNP enables the increase of their stability, functionality and biocompatibility, by adjusting the surface properties with the attachment of different type of molecules. It is important, however, that these modifications do not interfere with the properties of the AuNPs (DeLong et al., 2010; Conde et al., 2014). For biomedical purposes, AuNPs must be functionalized with other biomolecules, such as DNA/RNA oligonucleotides, fluorescent dye, peptides and/or antibodies, drugs and other molecules depending mostly on the final applications of AuNP-based systems (Conde et al., 2014).

For *in vitro* and *in vivo* applications, AuNPs should be stabilized against aggregation induced by biological fluids. This stablization allows acquiring long plasma half-lives for improvement of gene and drug delivery. For this purpose, PEG (poly(ethylene glycol)) is the most frequently used macromolecule since it was the advantage to be considered nontoxic and was approved for internal use in humans by Food and Drug Administration (FDA) (Owens III and Peppas, 2006; DeLong et al., 2010; Conde et al., 2014). The attachment of PEG to the AuNP surface by a thiol group, which binds with great affinity to gold, prevents the adsorption of other molecules by steric effect, such as opsins. These plasma proteins are responsible for the recognition of foreign substances, including AuNPs, by macrophages and monocytes from reticuloendothelial system (RES), and consequently responsible for the rapid removal of nanoparticles from circulation. The mechanism of action by which PEG prevents opsonization and increases circulation time is based on the formation of a sterically hindered by the hydrophilic coating, creating a shield against the binding of opsins. Moreover, chain flexibility of PEG induces a flexible and rapidly change of conformation, making difficult the interaction of opsins with the surface of AuNPs (Owens III and Peppas, 2006; Jokerst et al., 2012). By avoiding the adsorption of this type of molecules, pegylated AuNPs (AuNP@PEG) became more stable in biological environments and acquired longer systemic circulation (Sperlinger et al., 2008; Dreaden et al., 2012; Conde et al., 2014).

In addition to PEG molecules, AuNPs may be conjugated with additional biomolecules. One approach to link biomolecules is based on chemical mechanisms, where amino groups on the biomolecules are covalent binding with free carboxyl groups at the end of spacer molecules by an EDC/sulfo-NHS coupling reaction (Dreaden et al., 2012; Conde et al., 2014). EDC is a zero-length crosslinking agent used for couple carboxyl groups to primary amines, which together with sulfo-NHS, an intermediary reaction stabilizer, allows the conjugation of two biomolecules linked by a stable amide bond (Grabarek and Gergely, 1990).

Through this functionalization, the PEG chains allow further attachment of other biomolecules as for example tumor markers, drugs and fluorescent dyes. The easy surface modification of AuNPs with such different moieties together with their remarkable optical properties make AuNPs outstanding platforms for the development of theranostic systems for multiple applications (Figure I.2) (Conde et al., 2012).

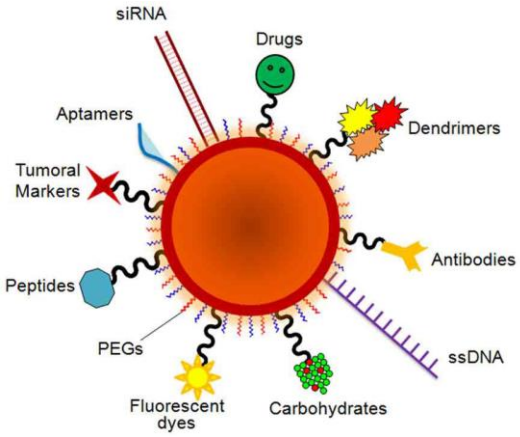

Figure I.2 - Schematic representation of a multifunctional AuNP. These multifunctional systems carry fluorescent dyes that are used for tracking and contrast agents. Nucleic acids (RNA and DNA) for gene silencing and colorimetric assays. Drug molecules and aptamers for delivery applications. PEG and antibodies to improve the AuNP circulation and targeting (Conde et al., 2014).

1.2.3. GOLD NANOPARTICLES IN NANOMEDICINE

Multifunctional AuNPs have been studied for theranostic applications, combining imaging, diagnostics and therapy. The development of these new systems aims to overcome the problems related to traditional drug delivery and therapeutic approaches, including inefficient delivery of the therapeutic agent, and inability to overcome biological barriers. Moreover theranostic nanomedicines allowed a noninvasive assessment of drug delivery and release, in combination with evaluation of therapeutic response and target site accumulation (Lammers et al., 2011; Cabral and Baptista, 2014; Vinhas et al., 2015).

One of the main challenges regarding drug delivery is related to the targeting of the nanosystems to the exact region of interest. In general, particles used in nanomedicine systems are known to achieve the pathological region either by passive or active targeting. The passive targeting of AuNPs is based on the enhanced permeability and retention effect (EPR), a property by which nanoparticles tend to accumulate more in tumor tissues than in normal ones. This effect occurs due to abnormal physiological characteristics of unhealthy tissues caused by the rapidly growth of tumor cells. This increased rate of growth became dependent of a rapidly blood supply, and the formed vessels have low vasculature with large fenestrations, allowing the extravasation of AuNPs to the interstitial space. Moreover, the decreased lymphatic drainage, characteristic of solid tumors, results in local accumulation of AuNPs. Usually, to increase this natural tendency of nanoparticles to accumulate in cancer tissues, nanosystems are functionalized with selective targeting agents - active targeting. Antibodies, DNA/RNA, folic acid and proteins are some examples of targeting agents, and the choice relies only on the desirable cell target and its biomarkers (Lammers et al., 2011; Vigderman and Zubarev, 2013; Cabral and Baptista, 2014).

AuNPs had been used in a diverse number of areas, such as *in vitro* assays, *in vitro* and *in vivo* imaging, cancer therapy and drug delivery. Oligonucleotide capped AuNPs had been used for nucleotide and protein detection using differently characterized mechanisms, including colorimetric detection using UV-visible spectroscopy and atomic force microscopy (AFM) (Cai et al., 2008). Moreover, AuNPs had been used as imaging agents for *in vitro* and *in vivo* imaging due not only to their intrinsic unique optical properties but also through their ability to be conjugated with contrast agents. Light scattering imaging, x-ray computed tomography (CT), surface-enhanced Raman spectroscopy (SERS) and magnetic resonance imaging (MRI) are some examples of imaging modalities that can use AuNPs as contrast agents (Lammers et al., 2011; Cabral and Baptista, 2014). In cancer therapy area, AuNPs had been used in photothermic therapy for destruction of cancer cells caused by increasing the intracellular temperature up to 70-60 induced by light absorption by AuNPs (Zharov et al., 2006). Additional AuNPs functionalized with small molecules, including TNF-α, tamoxifen and doxorubicin, have been for drug delivery and anti-cancer therapeutics (Cai et al., 2008; Cabral and Baptista, 2014).

More recently, several AuNPs based systems had been used for theranostic applications. In Table I.1 are listed some examples of AuNP based systems.

Table I.1 - Examples of AuNPs used in theranostic applications. Adapted from Cabral and Baptista, 2014; Vinhas et al., 2015.

AuNP type	AuNP Size	Therapeutic agent	Imaging agent	Targeting type	Reference
Spherical	12 nm	Radiation - DNA damage	CT imaging	Passive	(Joh et al., 2013)
Spherical	20 - 40 nm	Paclitaxel	Fluorescence	Biotin	(Heo et al., 2012)
Spherical	30 nm	Doxorubicin	CT imaging	Antigen RNA aptamer	(Kim et al., 2010)
Spherical	90 nm	Cetuximab	SERS imaging	Cetuximab (anti-EGFR)	(Mahmoudi et al., 2011)
Spherical	14 nm	siRNA	-	siRNA	(Conde et al., 2013)
Rods	72 nm x 35 nm (length x diameter)	siRNA	Light scattering	Passive	(Zhang et al., 2013)
Hollow spheres	52 nm	Doxorubicin	PET imaging	Passive	(You et al., 2010)

AuNPs have demonstrated to be a powerful tool for biomedical applications. However, these AuNP based systems have shown some limitations. Even though AuNPs are considerable biocompatible, their toxicity is dependent on several factors, including size, shape and surface functionalization, and because of that, every gold nanosystem should be properly characterized regarding their toxicity and

biocompatibility. In order to continue to develop these nanosystems and translate them to clinical approaches, a crucial point is yet necessary to understand - the mechanism by which AuNPs interact with biological systems, in particular with living cells (Cabral and Baptista, 2014; Oh and Park, 2014).

2. INTERNALIZATION OF GOLD NANOPARTICLES

Inappropriate delivery of therapeutic agents by traditional approaches led to inefficient therapeutics. As response, nanomedicine has led to the improvement of this therapeutics, by developing multifunction AuNPs as vectors for drug delivery, diagnostics and imaging applications (Cabral and Baptista, 2014). For drug delivery applications, AuNPs must interact with a specific cell population or with a specific intracellular compartment. To improve the delivery of therapeutic agents with AuNPs, their pharmacokinetics and biocompatibility must be first understood. Furthermore, it is necessary to keep in mind that each AuNP conjugate has unique properties that are directly related to the biocompatibility of AuNPs (Sahay et al., 2010; Cabral and Baptista, 2014).

Therefore, it has become increasingly necessary to understand how AuNPs interact with living cells and biological systems, i.e. the internalization mechanism of AuNPs (Cabral and Baptista, 2014; Oh and Park, 2014). Moreover, it is important to study how to direct AuNPs to a specific intracellular compartment depending on their final application. The study of cellular uptake of these nanomaterials is essential for assessing nanoparticle toxicity, to learn how to improve the accumulation of AuNPs in cells and tumors, and more important how to design more efficient nanoparticles (size, shape and surface chemistry) (Chithrani et al., 2006). The ability to control and manipulate the accumulation of these nanoparticles inside a cell can improve diagnostic and therapeutic efficiency (Chithrani and Chan, 2007). In order to advance nanotechnology for biomedical purposes, quantitative and qualitative studies on internalization mechanism of AuNPs are essential. Research suggests that cellular uptake of nanomaterials is dependent on their physicochemical characteristics, including size, shape and surface chemistry, as well on cell type (Sahay et al., 2010; Oh and Park, 2014).

2.1. FACTORS AFFECTING ENDOCYTOSIS OF GOLD NANOPARTICLES

2.1.1. SIZE

The size of AuNPs plays an important role in their cellular uptake. It has been demonstrated that AuNPs with diameter of 50 nm present higher cellular uptake rate when compared with smaller and larger nanoparticles (Chithrani et al., 2006). This optimum particle size is assumed to be due to a competition between the diffusion kinetics of membrane receptors and the process of membrane wrapping involved in endocytosis. The diffusion kinetics refers to the time necessary for the recruitment of plasma membrane receptors, and the process of membrane wrapping is related to the free energy required for the nanoparticles internalization. Therefore, smaller particles (< 50 nm) will not yield enough free energy for membrane wrapping, requiring them to cluster together to be internalized. On the other hand, for larger particles (> 50 nm) the wrapping time is slower due to a slower diffusion of plasma membrane

receptors (Chithrani and Chan, 2007; Zhao et al., 2011). However, to determine the influence of nanoparticles size in their cellular uptake with accuracy, stability and uniformity of size distribution of AuNPs must be guaranteed (Chithrani, 2010; Sahay et al., 2010).

2.1.2. SHAPE

AuNPs' shape is another property that influences their cellular uptake. A simple comparison between spherical AuNPs and gold nanorods with similar sizes demonstrated that spherical AuNPs are more easily internalized than rod-shaped AuNPs. This circumstance can be attributed to a longer time of membrane wrapping during rod-shaped particles cellular uptake (Chithrani et al., 2006; Zhao et al., 2011).

2.1.3. SURFACE CHARGE

The nanoparticles surface charge can be determined by the biomolecules attached to their surface. AuNPs positively charged had higher uptake efficiency than neutral and negatively charged AuNPs (Cho et al., 2009). The positively charged nanoparticles stick to the negatively charge plasma membrane, improving the cellular uptake. Furthermore, the cellular uptake of AuNPs could be facilitated by the interaction with molecules at the membrane surface (Chithrani, 2010).

2.2. INTERNALIZATION MECHANISMS

Endocytosis is a crucial process used by all types of mammalian cells to communicate with the biological environment. This is an energy-dependent process through which cells internalize molecules and ions, namely nutrients. However, its function is not restricted to the uptake of nutrients and signaling molecules, playing an important role on cell motility and inter-cell communication (Canton and Battaglia, 2012; Oh and Park, 2014).

The traditional classification of endocytic pathways is divided into two broad categories - phagocytosis, the uptake of large particles (cell eating), and pinocytosis, the uptake of fluids and solutes (cell drinking). The division of pinocytosis pathways is still a topic under ongoing research. The latest division is based on the proteins and lipids involved in the uptake process, being sub-divided into clathrin-mediated endocytosis (CME) and clathrin-independent endocytosis (CIE). This last category is divided in caveolae-mediated endocytosis, macropinocytosis and clathrin/caveolae independent endocytosis (Sahay et al., 2010). Figure I.3 illustrates a schematic representation of the different internalization mechanisms.

Nevertheless, all of these endocytic pathways are centered in four basic steps: (1) specific binding at the cell surface, (2) plasma membrane pinching off and formation of vesicles, (3) roping of the resulting vesicle and (4) trafficking of the vesicle to cytoplasm (Canton and Battaglia, 2012).

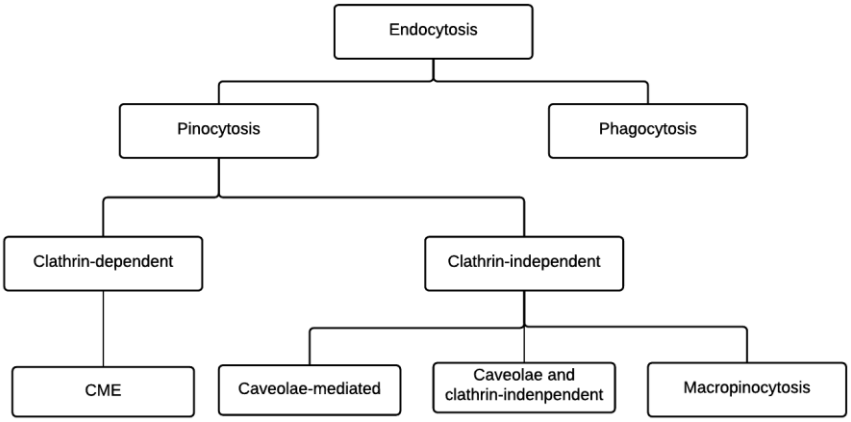

Figure I.3 - Classification of endocytosis based on the proteins that are involved in the initial uptake of particles and solutes. Adapted from (Sahay et al., 2010).

2.2.1. PHAGOCYTOSIS

Phagocytosis is an endocytic pathway only performed by specialized phagocytic cells, as macrophages and dendritic cells. This pathway is responsible for the internalization of pathogens, dead cells and cell debris and consists in a non-specific process to internalize fluids and large size particles, generally larger than 5 µm (Oh and Park, 2014). Mechanically, phagocytosis is initiated by the specific recognition of the particles by receptors at the surface of cell membrane. This recognition induces a membrane distortion that surrounds the particle, and engulfs it, resulting on the formation of a phagosome. Then this phagosome matures, fuses with lysosomes leading to degradation - see Figure I.4 (Ivanov, 2008; Sahay et al., 2010; Canton and Battaglia, 2012). One typical biological example of phagocytosis is the attained after the opsonization of foreign bodies and pathogens performed by immune cells (Canton and Battaglia, 2012).

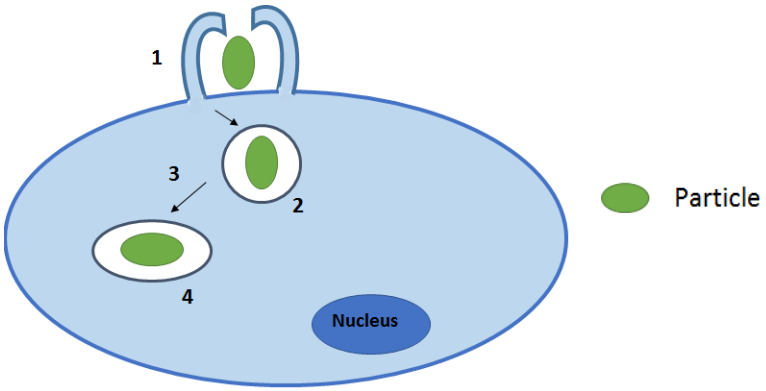

Figure I.4 - Schematic representation of phagocytosis. (1) Engulfment of large particles and fluids; (2) Particle ingested into phagosomes; (3) Fusion with lysosomes; (4) Phagolysosomes where particles are prone to degradation.

2.2.2. PINOCYTOSIS

2.2.2.1. CLATHRIN-MEDIATED ENDOCYTOSIS

Clathrin-mediated endocytosis is the most studied internalization mechanism, being the principal endocytic pathway responsible for nutrient uptake and allows the internalization of nanoparticles with size up to 150 - 200 nm (Sahay et al., 2010; Zhao et al., 2011). This process is initiated by the binding of particles at the membrane surface, triggered the formation of clathrin coated pits (CCP). After invagination, these coated pits are pinched off from the cell membrane by a small GTPase (dynamin), forming clathrin coated vesicles (CCV). Then clathrin present on these vesicles depolymerizes, and particles become clustered into endosomes. At this point, the endosome containing particles can fuse with lysosome and degradation is initiated. On the other hand, particles can be released to the cytosol and bypass degradation in some cases - see Figure I.5. Clathrin is a cytosolic protein responsible for the formation of the coated pits, in association with adaptor proteins (APs), which are responsible for coordinate the clathrin nucleation near the membrane location where particles are internalized (Ivanov, 2008; Sahay et al., 2010; Canton and Battaglia, 2012).

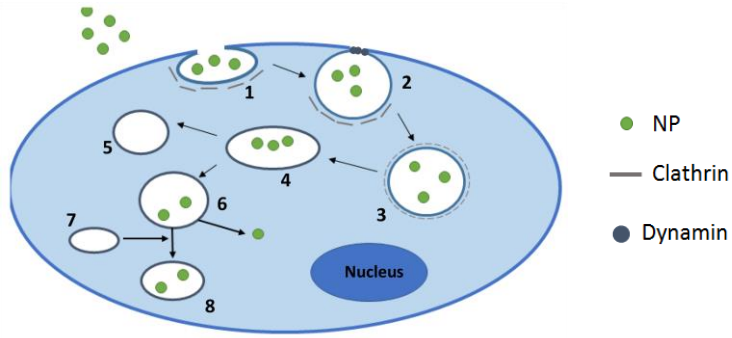

Figure I.5 - Schematic representation of clathrin-mediated endocytosis. (1) Uptake of nanoparticles into clathrin coated pits; (2) Clathrin coat pit pinched off from plasma membrane by dynamin; (3) Nanoparticle internalization into clathrin coated vesicles; (4) Endosomes; (5) Recycling of coat constituents; (6) Endosome release of nanoparticles; (7) Fuse with lysosome; (8) Degradation.

2.2.2.2. CAVEOLAE-MEDIATED ENDOCYTOSIS

Caveolae-mediated endocytosis is the most studied clathrin-independent internalization mechanism, being responsible for different biological functions, such as lipid regulation and vesicular transport (Canton and Battaglia, 2012). This process allows the internalization of nanoparticles with size up to 500 nm (Zhao et al., 2011). Caveolae are cholesterol-rich plasma membrane microdomains characterized by the presence of the proteins caveolin-1 and caveolin-2. The internalization of particles is initiated by the formation of flask-shaped invagination of the plasma membrane containing a striated coat of caveolin. After internalization, the vesicles turn into caveossomes containing the particles. Through this endocytic pathway, the internalized particles can be released to the cytoplasm or they can be set up for lysosomal degradation - see Figure I.6. This endocytic process seems to be more adequate for intracellular delivery and therapeutics since it usually can bypass lysosomal degradation, releasing

the endosomal cargo into the cytoplasm (Rejman et al., 2005; Sahay et al., 2010; Canton and Battaglia, 2012).

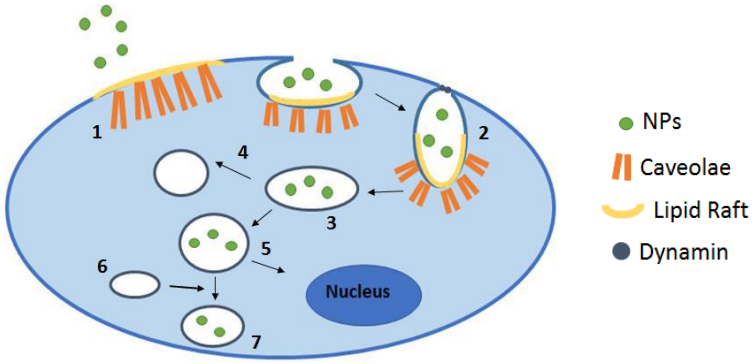

Figure I.6 - Schematic representation of caveolae-mediated endocytosis. (1) Binding of nanoparticles to lipid raft formed by caveolae; (2) Nanoparticle internalization into caveosomes that are pinched off from plasm membrane by dynamin; (3) Endosome; (4) Recycling of caveosome contains; (5) Endosome release of nanoparticles; (6) Fuse with lysosome; (7) Degradation.

2.2.2.3. MACROPINOCYTOSIS

Macropinocytosis is a clathrin/caveolae independent pathway, which is triggered by the tyrosine kinase receptor activation by growth factors (Sahay et al., 2010). This endocytic mechanism can internalize particles with size up to 5 µm (Zhao et al., 2011). This process comprises the engulfment of a large quantity of external fluid through the formation of waving sheet-like extensions of the plasma membrane, forming large vesicles called macropinosomes - see Figure I.7 (Sahay et al., 2010).

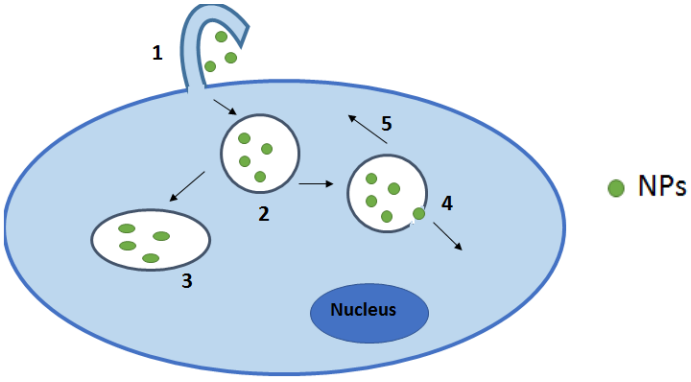

Figure I.7 - Schematic representation of macropinocytosis. (1) Engulfment of nanoparticles by ruffling of the plasma membrane; (2) Nanoparticle internalization into macropinosomes; (3) Lysosomal degradation; (4) Leakiness of nanoparticles into the cytosol; (5) Recycling.

2.3. ASSESSMENT OF INTERNALIZATION MECHANISMS

Currently, three different methods can be used to study the internalization mechanism of nanoparticles: (1) colocalization of intracellular nanoparticles with endocytic markers (Balasubramanian et al., 2009) (2) knockdown of specific endocytic proteins by siRNA (Mayor and Pagano, 2007) and (3) specific exclusion of internalization pathway by endocytic inhibitors.

The assessment of colocalization of intracellular nanoparticles is based on differential labeling of intracellular organelles and compartments, such as endosomes, lysosomes, caveolae and clathrin-coated pits. However, false colocalization can be obtained if the fluorescent markers show continuous areas of fluorescence that overlap with fluorescent signaling from other marker (Iversen et al., 2011).

The use of siRNA for knockdown specific endocytic proteins has been used to study a specific endocytic pathway. Nevertheless, the siRNA treatment may be considered time consuming since protocols can take 2-5 days and may result in undesirable cellular changes that can negatively influence the results. Moreover, the down-regulation of one internalization mechanism can lead to up-regulation of another endocytic pathway (Sahay et al., 2010; Iversen et al., 2011).

Although the previous two methods have been performed, the employment of endocytic inhibitors continues to shows several advantages over the molecular biological methods, including exposure of inhibitors to cells for a short period of time (30 min - 1 h), the knowledge that all cell are equally affected by inhibitors, and the fact that the use of endocytic inhibitors are the most affordable approach (Ivanov, 2008). It is known, however, that the use of these inhibitors to study internalization mechanisms of nanoparticles is based on the assumption that each inhibitor has a specific influence on a single endocytic pathway.

Chlorpromazine and potassium depletion are two different approaches frequently used for the inhibition of clathrin-mediated endocytosis. Chlorpromazine is an amphipathic molecule responsible for the loss of clathrin and adaptor protein on the cell surface and consequently the impossibility to assemble the clathrin coated pits at the plasma membrane surface. The method of potassium depletion consists in a hypotonic treatment followed by incubation in potassium-free medium. This approach is responsible for removable of clathrin lattices from the plasma membrane (Ivanov, 2008; Vercauteren et al., 2010).

Filipin and nystatin are two inhibitors of caveolae-mediated endocytosis. These inhibitors interact with cholesterol, changing the properties of cholesterol-rich membrane domains, and as result interfering with the formation of flask-shaped invagination responsible for the uptake of nanoparticles (Ivanov, 2008).

Amiloride and wortmannin are able to inhibit two different mechanisms of the macropinocytosis pathway. Amiloride interferes with sodium-proton exchange and wortmannin inhibits the phoinositide 3-kinase (PI3K) (Ivanov, 2008).

Although the use of endocytic inhibitors has several advantages, their specific to a single internalization route has been questioned (Ivanov, 2008; Sahay et al., 2010; Vercauteren et al., 2010; Iversen et al., 2011). Therefore, for more straight results, combination of different methods should be considered.

3. OBJECTIVES

The use of nanoparticles for biomedical applications has increased in the current times. In order to improve the efficiency of intracellular delivery by nanoparticles, the biological interaction between nanoparticles and cells needs to be fully understood. The main goal of this work was to assess the internalization mechanism of AuNPs, a nanosystem whose interest has goon, by fluorescent spectroscopy and microscopy. In order to achieve this objective, several tasks were set:

i. Synthesis of gold nanoparticles.
ii. Functionalization and characterization of AuNPs with PEG and a fluorescent dye.
iii. Evaluation of the uptake of the functionalized AuNPs as function of time.
iv. Assessment of the internalization mechanism of the functionalized AuNPs.
v. Analysis of the effect of the functionalized AuNPs on the proliferation rate and viability of mammalian cells.

II. MATERIALS AND METHODS

1. SYNTHESIS OF GOLD NANOPARTICLES

The 14 nm AuNPs were synthetized by the citrate reduction method adapted from Lee and Meisel (Lee and Meisel, 1982), as described elsewhere (Conde et al., 2012).

All glass materials used during the synthesis were previously immersed in *aqua regia* (1:3 HNO_3:HCl) overnight and then washed with distilled H_2O and mili-Q H_2O (18.2 MΩ.cm^{-1} at 25 °C). All solutions were prepared in mili-Q H_2O.

In a 500 mL round bottom flask, 250 mL of 1 mM $HAuCl_4$ (Sigma, MW 393.83 Da) were brought to boil with vigorously stirring. When in reflux, 25 mL of 38.8 mM of sodium citrate (Sigma, MW 294.10 Da) were rapidly added and kept refluxing for 20 minutes with continuous stirring. After that, the solution was left to cool at room temperature (RT) with continuous stirring and then stored in a 500 mL Erlenmeyer, protected from light, at RT.

Synthetized AuNPs were characterized by Transmission Electron Microscopy (TEM) and Dynamic Light Scattering (DLS), and their concentration was determined by UV-visible Spectroscopy.

2. FUNCTIONALISATION OF GOLD NANOPARTICLES

2.1. AuNP@PEG

AuNPs were functionalized with a hetero-functional PEG (poly(ethylene glycol)) molecule (Iris BIOTECH, MW 458.57 Da) containing a thiol group at one end and a carboxyl group at the other end of the molecule - HS-EG(8)-COOH.

In order to achieve the complete saturation of PEG on the surface of AuNPs, increased concentrations of PEG were added to a fixed amount of AuNPs. Briefly, 10 nM of AuNPs were mixed with a range of concentration of 0 - 0.1 mg.mL^{-1} PEG and 0.028 % (v/v) SDS (sodium dodecyl sulfate) (Sigma, MW 288.38 Da) in aqueous conditions. Then the samples were left 16 hours at RT with continuous stirring on a GLF 3016 shaker. To remove the excess of PEG chains that did not functionalized the AuNP surface, the mixtures were centrifuged three times for 45 minutes at 14000 g, at 4°C, where the supernatants were removed to new eppendorfs and replaced by mili-Q H_2O. The three resulting supernatants were also centrifuged under the same previously conditions, and then the remaining thiolated chains of PEG were quantified by Ellman's assay.

In Ellman's assay the thiol groups presented in the supernatants react with DTNB (5,5'-dithiobis-(2-nitrobenzoic acid)), (Sigma, MW 396.35 Da) giving a yellow solution which can be quantified in a spectrophotometer, measuring the absorbance at 412 nm.

This assay was performed on a 96-well plate, by mixing 200 µL of the supernatant with 100 µL of 0.5 M phosphate buffer pH 7.0 - prepared by the addition of 288.55 mM Na_2HPO_4 (Sigma, MW 141.96 Da)

and 211.45 mM NaH_2PO_4 (Sigma, MW 119.98 Da) - and 7 µL of 2 $mg.mL^{-1}$ DTNB prepared in 0.5 M phosphate buffer pH 7.0. After this, the plate was left at RT for 10 minutes, and then the absorbance was measured from 290 nm to 600 nm in an Infinite M200 microplate reader (Tecan, Switzerland). Under the same conditions, a calibration curve was set in a range of 0 - 0.5 $mg.mL^{-1}$ of PEG, in which the supernatant was replaced by a standard solution of PEG at increased concentrations. The excess thiolated chains in each supernatant can be quantified by interpolating the calibration curve.

In the current work, the AuNPs were functionalized with 0.01 $mg.mL^{-1}$ of PEG.

The AuNP@PEG were characterized by DLS and, and their concentration determined by UV-visible spectroscopy.

2.2. AuNP@PEG@TAMRA

AuNP@PEG were further functionalized with a fluorescent dye, TAMRA (tetramethylrhodamine cadaverine) (Life Technologies, MW 514.623 Da) by EDC (1-ethyl-3-(3-dimethylaminopropyl)-carbodiime) and sulfo-NHS (sulfo-hydroxysuccinimide) coupling reaction (Figure II.1).

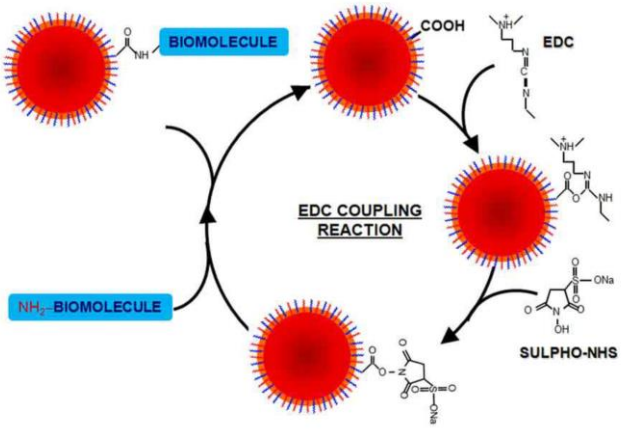

Figure II.1 - Reaction scheme of EDC coupling reaction. In presence of sulfo-NHS, EDC converts carboxyl groups to amine-reactive sulfo-NHS esters. The addition of sulfo-NHS stabilizes the amine reactive intermediated (Conde et al., 2014).

For this functionalization, a master mix was prepared containing 21 nM AuNP@PEG, 1.25 $mg.mL^{-1}$ sulfo-NHS (Sigma, MW 217.13 Da) and 0.312 $mg.mL^{-1}$ EDC (Sigma, MW 191.70 Da) in 2.5 mM MES buffer pH 5.9 (Sigma, MW 195.24 Da). The master mix was incubated for 30 minutes at RT with continuous stirring, and then centrifuged at 14000 g for 30 minutes at 4°C. The supernatant was removed, and replaced by 2.5 mM MES buffer pH 5.9, in equal volume. Then TAMRA was added to the mixture at a final concentration of 10^{-7} M, and the final mixture was incubated at RT for 16 hours with continuous stirring.

To remove the unbound TAMRA, the mixture was centrifuged 5 times for 45 minutes, at 14000 g and 4°C. All the supernatants were removed to new eppendorfs and replaced by 2.5 mM MES buffer pH 5.9

in equal volume, and later, supernatants were also centrifuged under the previous described conditions. Excess of TAMRA was quantified in all supernatants by fluorescent spectroscopy. The fluorescent intensity measurements were performed at RT using a Cary Eclipse Fluorescence spectrophotometer at excitation wavelength of 543 nm and recorded in a frequency range of 550 - 700 nm, at 600 nm/min with a photomultiplier potency of 600 V, using quartz cells with 1 cm of excitation path (105.254-QS, Hellma, Germany). Under the same conditions, a calibration curve was prepared in a range of 0 - 10^{-7} M of TAMRA in 2.5 mM MES buffer pH 5.9, and the fluorescent intensity was measured using the previous settings. Excess TAMRA was quantified by interpolating the calibration curve.

AuNP@PEG@TAMRA were characterized by and DLS and, their concentration determined by UV-visible spectroscopy, and fluorescent intensity was measured by fluorescent spectroscopy.

3. TEM ANALYSIS

TEM analysis were performed in Instituto de Ciência e Engenharia de Materiais e Superfícies (ICEMS/IST), Portugal, with a HITACHI H-8100 microscope operated at 200 kV. Samples were prepared by depositing 10 µL of the prepared colloidal suspensions in carbon copper grids, washed twice with 10 µL of milli-Q H_2O and air dried. Particles size and shape were determined by analyzing the TEM pictures using the image software ImageJ.

4. DLS ANALYSIS

The hydrodynamic diameter of all synthetized AuNPs was determined by DLS using a Nanoparticle Analyser SZ-100 (Horiba Scientific, Japan) at 25 °C, with a scattering angle of 90°. All AuNPs samples were prepared under sterile conditions, at a final concentration of 2 nM. For each sample 6 measures were performed.

5. UV-VISIBLE SPECTROSCOPY

All synthetized AuNP were characterized using an UV-visible spectrophotometer (UVmini-1240, Shimadzu, Germany). Absorbance measurements were carried out using 100 µL of volume quartz absorption cells with 1 cm optical path (105.202-QS, Hellma, Germany).

6. HUMAN CELL CULTURE

A549 human lung carcinoma cells were grown in Dulbecco's modified Eagle's medium (DMEM, Invitrogen) supplemented with 1 % (v/v) penicillin/streptomycin (10000 units/mL of penicillin, 10000 units/mL of streptomycin, Invitrogen), 10 % (v/v) heat inactivated fetal bovine serum (FBS, Invitrogen) and 1 % (v/v) of non-essential amino acids (NEA, Invitrogen). Cells were maintained in 75 cm^2 culture

flasks (SPL) in a CO_2 incubator (Sanyo, Japan) at 37 °C in a 99 % humidified atmosphere of 5 % (v/v) CO_2.

Cell culture medium was renewed at approximately 80 % of confluence. Briefly, culture medium was aspired, 2 mL trypsin (Invitrogen) were added and incubated for 5 minutes at 37 °C in a 99 % humidified atmosphere of 5 % (v/v) CO_2. After that, loss of cells adherence was confirmed using an inverted microscope (Nikon TMS), and 8 mL of DMEM were added to the culture flask to neutralize the trypsin. Approximately 1 mL of this solution was added to a new 75 cm^2 culture flask, containing 13 mL of DMEM, and maintained under the conditions previous described. The remaining cell solution was used in further assays or discarded.

7. UPTAKE STUDIES OF AuNP@PEG@TAMRA

7.1. EVALUATION OF THE UPTAKE KINETICS OF AuNP

In order to study the uptake kinetics of the functionalized AuNPs, uptake experiments were performed in A549 cells as function of time.

7.1.1. CELL COUNT ASSAY BY TRYPAN BLUE

The number of viable cells was assessed by trypan blue assay. Briefly, a solution containing 40 µL of 0.4 % (m/v) trypan blue (Sigma) and 10 µL of cell suspension was positioned on a hemocytometer (Hirschmann, Germany), and the number of viable cells was determined by visualization on an inverted microscope. Trypan blue is a blue dye that can trespass the plasma membrane of non-viable cells, which plasma membrane is more permeable (Strober, 2001). The resulting cell density was determined according to Equation II.1:

$$Nº\ of\ Viable\ Cells.mL^{-1} = \frac{\Sigma cells\ per\ quadrant}{4} \times 10^4\ (Chamber\ Volume) \times dilution\ factor \quad (\mathbf{II.1})$$

7.1.2. CELL SEEDING FOR AuNP@PEG@TAMRA

Subsequently to the determination of the number of viable cells, A549 cells were seeded at a density of 2.5 x 10^4 cells/well in a 24-well plate (SPL) in a total volume of 500 µL. Cells were maintained at 37 °C in a 99 % humidified atmosphere of 5 % (v/v) CO_2 for 24 hours prior to AuNP incubation. After 24 hours, when cells reached monolayer, medium was removed, and 300 µL of 10 nM AuNP@PEG@TAMRA prepared in DMEM were added to each well.

Cells were incubated with AuNPs for 1, 3, 6, 12 and 24 hours, and were maintained at 37 °C in a 99 % humidified atmosphere of 5 % (v/v) CO_2.

The cellular uptake kinetics of this AuNPs was assessed by fluorescence spectroscopy and microscopy.

7.2. FLUORESCENCE SPECTROSCOPY

After each period of incubation, culture medium containing AuNPs was removed, and cells were washed twice with bicarbonate Krebs-Ringer buffer (Salomon and Ehrhardt, 2010) (KRB, composed of 15 mM HEPES, 116.4 mM NaCl, 5.4 mM KCl, 0.78 mM NaH_2PO_4, 25 mM $NaHCO_3$, 1.8 mM $CaCl_2$, 0.81 mM $MgSO_4$ and 5.55 nM glucose, pH 7.4) and lysed with a 1 % (v/v) solution of Triton X-100 prepared in KRB buffer, pH 7.4.

The fluorescence intensity of each lysate was measured by fluorescence spectroscopy. All measurements were performed at RT, at excitation wavelength of 543 nm and recorded in a frequency range of 550 - 700 nm, at 30 nm/min with a photomultiplier potency of 800 V.

7.3. FLUORESCENCE MICROSCOPY

A549 cells were seeded at a density of 1 x 10^5 cells/well in a 24-well plate in a total volume of a 500 µL. Cells were left to growth for 24 hours as described in Section II.7.1.2. Prior to cell seeding sterilized cover slips were placed at the bottom of each well. After 24 hours, cells were incubated as described in Section II.7.1.2, for the same period of time.

After each incubation period, culture medium was removed, and cells were washed twice with PBS 1x, and then fixed with 4% solution of paraformaldehyde in PBS for 15 minutes. Then, cells were washed three times with PBS 1x and mounted in ProLong Gold Antifade Reagent with DAPI (Invitrogen) to allow nuclear staining. Slides were visualized in a Olymous BX51 fluorescent microscope with an attached Olympus DP50 camera.

7.4. ICP-MS ANALYSIS

The quantification of gold in cell lysates was evaluated by ICP-MS, performed at Laboratório de Análises - Serviço de Espectroscopia de Emissão Atómica at Departamento de Química at FCT-UNL.

After cellular uptake, cell lysates were digested in fresh *aqua regia* for 48 hours. All samples were measured only once.

8. INHIBITION STUDIES WITH PHARMACOLOGICAL INHIBITORS

8.1. SINGLE ACTION OF INHIBITION AGENTS

A549 cells were seeded at the same density and conditions as described in Section II.7.1.2.

After 24 hours, cells were pre-treated with following endocytic inhibitors in DMEM for 30 minutes at 37°C in a 99 % humidified atmosphere of 5 % (v/v) CO_2 - 300 nM wortmannin (Sigma, MW 428.43), 1.53 µM filipin III (Sigma, MW 654.8), 28.14 µM chlorpromazine hydrochloride (Sigma, MW 355.3) and 1.5 mM amiloride hydrochloride (Sigma, MW 266.1). Subsequently, culture medium was removed and replaced

with a solution containing 10 nM of AuNP@PEG@TAMRA in combination with each individual inhibitor (continuous inhibition).

The inhibition studies were carried out for 1, 3 and 6 hours. After these periods, the AuNP uptake was assessed by fluorescence spectroscopy and microscopy, and by ICP analysis, as described in Section II.7.2, Section II.7.3 and Section II.7.4, respectively, - see Figure II.2.

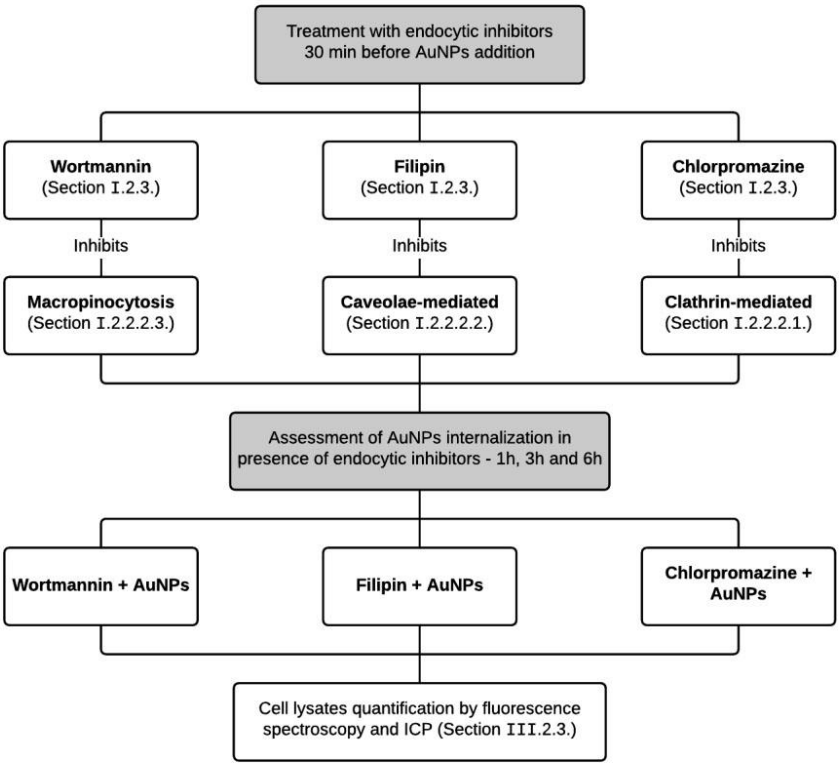

Figure II.2 - Schematic representations of the experimental protocol of the inhibition studies regarding the single action of inhibitions agents. Treatment with endocytic inhibitors 30 min before the addition of AuNPs, followed by the assessment of AuNPs internalization in presence of endocytic inhibitors by fluorescent spectroscopy and ICP.

8.2. COMBINATORY ACTION OF INHIBITION AGENTS

A549 cells were seeded at the same density and conditions as described in Section II.7.1.2.

After 24 hours, cells were pre-treated with four combinations of the previous endocytic inhibitors in DMEM for 30 minutes at 37 °C in a 99 % humidified atmosphere of 5 % (v/v) CO_2 - wortmannin + filipin, wortmannin + chlorpromazine, filipin + chlorpromazine and wortmannin + filipin + chlorpromazine. Subsequently, the culture medium was removed and replaced with a solution containing 10 nM of AuNP@PEG@TAMRA in addition with each inhibitor combination (continuous inhibition).

The inhibition studies were carried out for 1, 3 and 6 hours. After these periods, the AuNP uptake was assessed by fluorescence spectroscopy and microscopy, and by ICP analysis, as described in Section II.7.2, Section II.7.3 and Section II.7.4, respectively, - see Figure II.3.

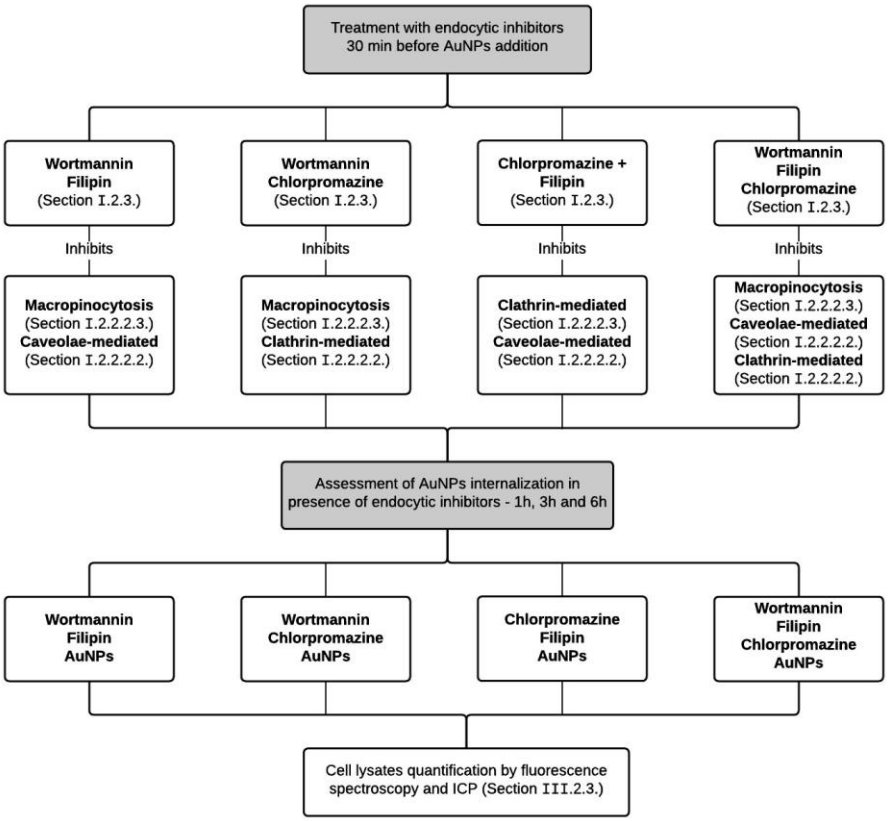

Figure II.3 - Schematic representations of the experimental protocol of the inhibition studies regarding the combinatory action of inhibitions agents. Treatment with endocytic inhibitors 30 min before the addition of AuNPs, followed by the assessment of AuNPs internalization in presence of endocytic inhibitors by fluorescent spectroscopy and ICP.

9. CELL VIABILITY AND CYTOTOXICITY STUDIES OF AUNP FORMULATION AND PHARMACOLOGICAL INHIBITORS

9.1. MTS ASSAY

The cytotoxicity of the AuNP formulation and endocytic inhibitors was evaluated using the MTS assay (CellTiter 96® Aqueous Non-Radioactive Cell Proliferation Assay, Promega, USA).

MTS (3-(4,5-dimethylthiazol-2-yl)-5-(3-carboxyphenyl)-2-(4-sulfophenyl)-2H-tetrazolium) and PMS (phenazine methosulfate) assay is a colorimetric method for determining the number of viable cells. Briefly, the MTS compound in presence of PMS is reduced by metabolically active cells into formazan, a colored product which absorbance can be measured at 490 nm, see Figure II.4.

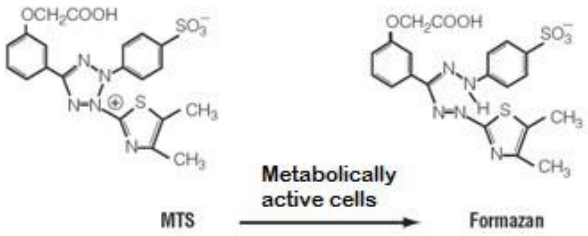

Figure II.4 - Reaction scheme of MTS assy. In presence of metabolically active cells, MTS is converted to formazan by metabolically enzymes, a brown product, which formation can be measured spectroscopically.

Therefore, the quantity of formazan produced is directly proportional to the number of metabolically active cells, and so, the cell viability of each sample can be obtained according to Equation II.2.

$$Cell\ Viability\ (\%) = \frac{Sample\ absorbance\ at\ 490\ nm}{Control\ absorbance\ at\ 490\ nm} \times 100 \qquad (II.2)$$

A549 cells were seeded at a density of $7.5x10^3$ cells/well in a 96-well plate. Cells were left to growth for 24 hours at 37 °C in a 99 % humidified atmosphere of 5 % (v/v) CO_2. After 24 hours, cells were incubated with a range of AuNP concentrations (0 - 20 nM) for 24 hours at 37°C in a 99 % humidified atmosphere of 5 % (v/v) CO_2. Subsequently to this period of incubation, culture medium containing the AuNPs was removed and replaced by fresh medium, and cells were incubated for another 24 hours at 37 °C in a 99 % humidified atmosphere of 5 % (v/v) CO_2. After that, a mixture of DMEM, MTS and PMS in a ratio of 100:20:1 was added to each well and cells were incubate for 40 minutes at 37°C in a 99 % humidified atmosphere of 5 % (v/v) CO_2. Then the absorbance was measured by Tecan Infinite F200 Microplate Reader (Tecan, Switzerland) at 490 nm. The percentage of cell viability for each sample was obtained accordingly to Equation II.2.

To assess the cytotoxicity of the different endocytic inhibitors, A549 cells were seeded at a density of $7.5x10^3$ cells/well in a 96-well plate. Cells were left to growth for 24 hours at 37°C in a 99 % humidified atmosphere of 5 % (v/v) CO_2. After 24 hours, cells were incubated with AuNP and different endocytic inhibitors as described in Section II.8.1. Subsequently to this period of incubation, the procedure is equal to the one described above.

9.2. CELL COUNT BY TRYPAN BLUE

As mentioned in Section II.7.1.1, the number of viable cells can be assess by the trypan blue assay. In order to assess the cell viability in presence of the endocytic inhibitors and AuNPs, A549 cells were treated with the different inhibitors and AuNPs as described in Section II.8.1. After each incubation period, cells were washed once with PBS 1x, 200 μL of trypsin was added and incubate for 5 minutes

at 37 °C in a 99 % humidified atmosphere of 5 % (v/v) CO_2. Next, 300 μL of culture medium was added and the number of viable cells was determined as described in Section II.7.1.1.

9.3. CELL COUNT BY NUCLEUS STAINING

A549 cells were incubated as mentioned in Section II.8.1. After each incubation period, culture medium was removed, and cells were washed twice with PBS 1X, and then were fixed with 4% solution of paraformaldehyde in PBS for 15 minutes. Then, cells were washed three times with PBS 1x and mounted in ProLong Gold Antifade Reagent with DAPI (Invitrogen) to allow nuclear staining.

In order to assess the cell viability, every nucleus with normal morphology was counted.

10. STATISTICS ANALYSIS

Statistical significance of all data was verified by One-way ANOVA. The Tukey method allowed to determined statistical significant differences between the cellular uptake using different endocytic inhibitors. This analysis was performed with GraphPad Prism 6.0 (GraphPad Software, Inc) and results were considered statistical significant for $P < 0.05$.

III. RESULTS AND DISCUSSION

1. GOLD NANOPARTICLES

Noble nanoparticles are considered a key tool to a variety of biomedical applications, including diagnostic assays (Baptista et al., 2008; Selvan, Yang et al., 2010) and drug and gene delivery (Yavuz et al., 2009). In particular AuNP-based systems can be used simultaneously for diagnostic and therapeutic - theranostics (Xie et al., 2010). This noble metal exhibits broad distinctive characteristics, such as great optical properties, easy to synthetize and easy surface functionalization with biocompatible polymers that enhance their *in vivo* circulation necessary for therapeutic applications (Bhattacharyya et al., 2011). Therefore, AuNPs are becoming an interesting system and so the understanding of their internalization mechanism and cellular interactions is essential to enhance the expected outcome.

1.1. SYNTHESIS AND CHARACTERIZATION

Stable AuNPs were successfully synthetized by the citrate reduction method (Lee and Meisel, 1982). In this method, citrate molecules are used both as reduction agent and capping agent. In this work, 14 nm spherical AuNPs synthetized were characterized by UV-visible spectroscopy, dynamic light scattering (DLS) and transmission electron microscopy (TEM).

UV-visible spectroscopy allows the characterization of the AuNPs optical properties as result of their surface plasmon resonance (SPR). The SPR effect depends on the size, shape and inter-particle distance, and also on the surrounding media (Hu et al., 2006). This property gives AuNP high absorption coefficients with a typical SPR absorption band centered around 519 nm for spherical 14 nm AuNPs (Jain et al., 2006). As Figure III.1C shows, the obtained AuNP dispersion displayed a single absorption band with a maximum plasmon peak at 518 nm, typical of spherical 14 nm AuNPs. Also, the obtained absorption spectrum is symmetrical at the SPR peak (518 nm) indicating the presence of monodisperse spherical AuNPs in the colloid solution (Shi et al., 2012). This data also allows the quantification of the AuNPs concentration by the Lambert-Beer law, assuming an absorption coefficient of 2.33×10^8 $M^{-1}.cm^{-1}$ for the SPR maximum peak (Baptista et al., 2005).

Dynamic light scattering (DLS) is a technique that gives complementary information about AuNPs diameter. This technique is based on the fact that small particles in suspension undergo thermal Brownian motion induced by collisions between the particles and solvent molecules. When the particles are irradiated with a laser, the intensity of the scattered light oscillates over time, which is dependent upon the particles size. The differential light scattered is related to the AuNPs hydrodynamic diameter that depends on the surrounding media and on the molecules at the AuNP surface (Tomaszewska et al., 2013). DLS characterization showed that the citrate capped AuNPs had a diameter of 18.17 ± 0.64 nm. This value is higher than the value assumed by the absorption spectrum (c.a. 14 nm), which can be explained by the capping molecules of citrate the lead to an increased hydrodynamic diameter.

Moreover, DLS analysis also provides information about the AuNP size distribution through the polydispersity index. The AuNPs synthetized showed a polydispersity index of 0.17 ± 0.06 which indicates a high monodisperse population.

The final technique used to characterize the AuNPs was transmission electron microscopy (TEM), providing direct visualization of morphology and size distribution profile of AuNPs. TEM images (Figure III.1A and Figure III.1B) confirmed the high monodispersing and spherical shape of the synthetized nanoparticles. In order to determine the AuNP size, a total of 262 AuNPs were measured using the software Image J. AuNPs showed an average diameter of 13.66 ± 2.10 nm, which was in accordance to UV-visible characterization.

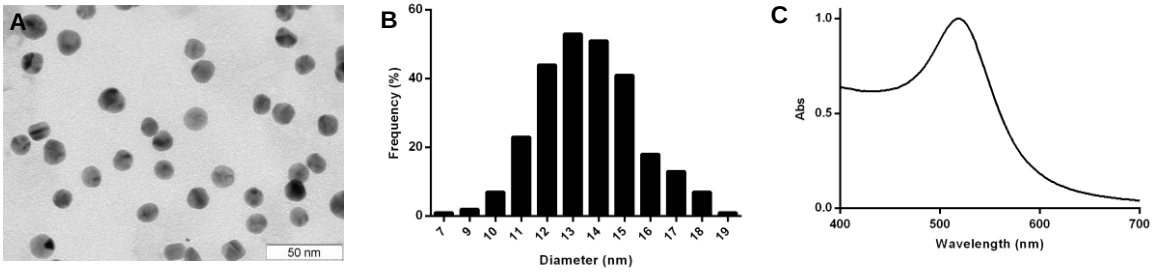

Figure III.1 - Characterization of the synthesized AuNPs. (A) Transmission electron microscopy (TEM) imaging (scale bar 50 nm); (B) Size distribution of AuNPs from counting 262 particles; (C) UV-visible spectrum of AuNPs in wavelength range of 400 - 700 nm, with a maximum absorption of the SPR band centered at 518 nm.

1.2. FUNCTIONALIZATION AND CHARACTERIZATION

1.2.1. POLY(ETHILENE) GLICOL

In order to increase biocompatibility, stability and also provide further chemical functionalization, the citrate capped AuNPs were coated with PEG molecules. This hydrophilic polymer creates an inert hydrophilic surface, preventing unspecific binding of other molecules, such as opsins. This is an important feature for *in vivo* applications (Sperling and Parak, 2010).

The citrate coated AuNPs were functionalized with a bi-functional PEG molecule (SH-EG(8)-COOH), with a thiol group at one end to be attached to the AuNP core, and a carboxyl group at the other end to enable further chemical functionalization. The final AuNP@PEG were coated with a 100% saturation of PEG molecules, corresponding 0.01 $mg.mL^{-1}$. The determination of the degree of saturation is in Appendix A1.

After functionalization, AuNP@PEG were characterized by UV-visible spectroscopy and DLS. By UV-visible spectroscopy is possible to notice a 2 nm shift of the SPR band from 518 to 520 nm, meaning an increasing in the AuNP size due to the attachment of the PEG molecules (Figure III.2). Moreover, a minor enlargement of the SPR band can be seen, which can indicate an enhancement of the polydispersity.

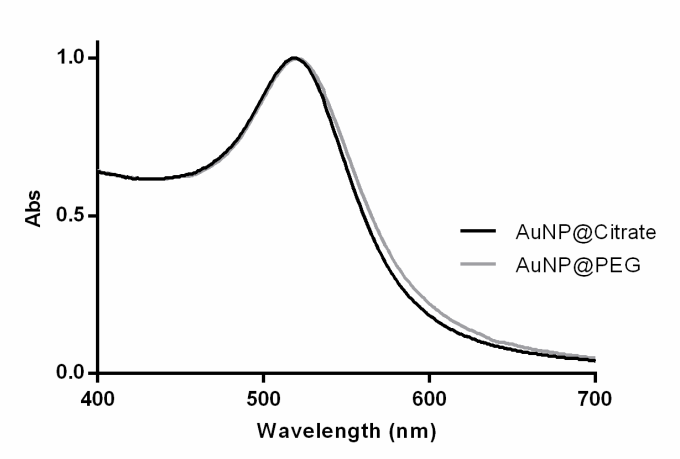

Figure III.2 - Characterization of the pegylated AuNPs by UV-visible spectroscopy. UV-visible spectrum of the previously synthetized AuNP@Citrate and AuNP@PEG, enlightening the SPR shift from 518 nm to 520 nm and the minor enlargement of the SPR band.

The DLS analysis determined an increase of the hydrodynamic diameter of 18.17 ± 0.64 to 21.78 ± 3.92 nm, a 3.61 nm increment that indicates a replacement of the citrate coat by a monolayer layer of PEG chains. Since the size of a single molecule of PEG is 3.25 nm (www.iris-biotech.de), it was expected an enhancement of hydrodynamic diameter in about 6.5 nm. However, DLS analysis only shows a 3.61 nm increase that can be due to the high flexibility of PEG chains that might influence the Brownian motion of the AuNPs. Also, the polydispersity index increased from 0.17 ± 0.06 to 0.21 ± 0.03, in concordance with the characterization by UV-visible spectroscopy.

1.2.2. TAMRA

In order to produce an AuNP able of been tracked by fluorescent spectroscopy and microscopy during cellular uptake, it was necessary to attached a fluorophore molecule to the AuNP@PEG previously synthetize. Therefore, the AuNPs were functionalized with TAMRA dye, a rhodamine-based fluorophore, by an EDC/NHS coupled reaction, taking advantage of carboxyl groups of PEG chains already attached to the AuNP surface, and primary amine groups from TAMRA dye.

Using EDC and sulfo-NHS, the TAMRA dye was linked covalently to the surface of AuNP@PEG, resulting in AuNP@PEG@TAMRA. AuNP@PEG@TAMRA were characterized by UV-visible spectroscopy, DLS, and fluorescent spectroscopy. Also the amount of TAMRA attached to the AuNP was achieved by fluorescent spectroscopy by interpolation of a calibration curve (Appendix A2). The conjugation of TAMRA to the AuNP@PEG results in a 1 nm SPR shift from 520 to 521 nm. This minor shift is not explicit by UV-visible spectroscopy as showed in Figure III.3. The AuNP@PEG and AuNP@PEG@TAMRA spectrums are almost coincident, which can mean that the attachment of TAMRA did not induce a significant increase on the diameter of the nanoconjugate. This evidence is also confirmed by the DLS analysis, where the hydrodynamic diameter shifts from 21.78 ± 3.92 to 22.52 ± 0.33 nm, a non-significant increase.

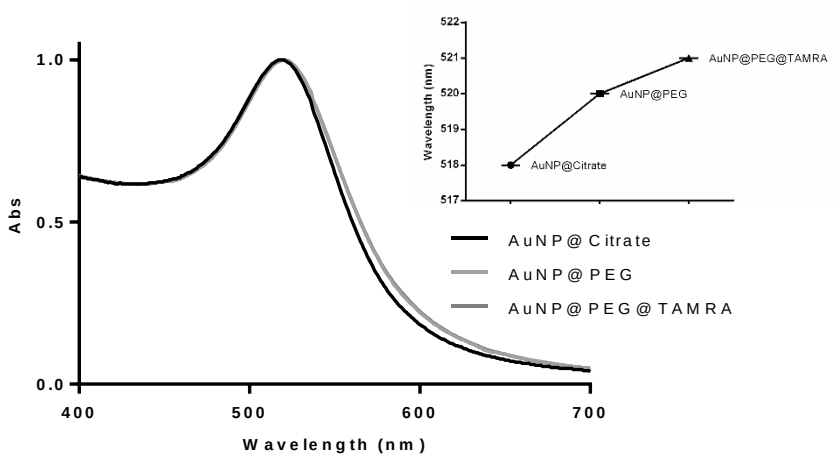

Figure III.3 - Characterization of AuNP@PEG@TAMRA by UV-visible spectroscopy. UV-visible spectrums of the synthetized AuNPs (AuNP@Citrate), AuNPs coated with PEG (AuNP@PEG) and coated with PEG and TAMRA (AuNP@PEG@TAMRA) in a wavelength range of 400 - 700 nm. Inset presenting the maximum of the SPR band shift through all functionalization.

This nanoconjugate was also characterized by fluorescent spectroscopy, in order to determine the number of TAMRA molecules attached to the AuNPs and to assess the fluorescent properties of AuNP@PEG@TAMRA. After quantification of the TAMRA molecules present in supernatants, a AuNP:TAMRA ratio of 1:4 ± 0.3 was achieved. Figure III.4 shows the fluorescent profile of the prepared AuNPs, which is indicative of the attachment of the TAMRA dye to the AuNP surface.

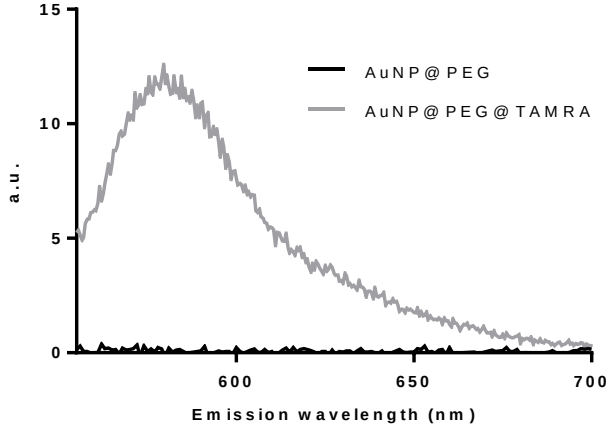

Figure III.4 - Characterization of AuNP@PEG@TAMRA by fluorescence spectroscopy. Emission spectrum of 5 nM of AuNPs coated with PEG (black line) and 5 nM of AuNPs coated with PEG and TAMRA (grey line) at excitation wavelength of 543 nm and recorded in a frequency range of 550 - 700 nm, at 30 nm/min with a photomultiplier potency of 800 V.

2. INTERNALIZATION OF GOLD NANOPARTICLES

In order to continue the development of AuNPs with improved therapeutic efficacy is necessary to acquire an intense knowledge of their interactions with living cells and biological systems. More precisely, the internalization mechanism by which AuNPs are taken up by cells with minimal toxicity.

2.1. KINETICS OF CELLULAR UPTAKE

As mentioned before, the characterization of the prepared AuNP@PEG@TAMRA showed the presence of fluorescent properties that make the formulation suitable for tracking during the cellular internalization by fluorescent spectroscopy. In this work, spectroscopy and microscopic techniques have been selected to evaluate the cellular uptake - fluorescent spectroscopy and ICP-MS to quantification two different elements of the nanoconjugate, and fluorescent microscopy to enable the visualization of AuNP localization inside cells (Elsaesser et al., 2010; Rothen-Rutishauser et al., 2014).

To determine the kinetics profile of the cellular uptake of this formulation, A549 cells (human lung carcinoma) were incubated with 10 nM of AuNP@PEG@TAMRA for 1 - 24 h. After the incubation period, A549 were lysate as mentioned in Section II.7.2, and the fluorescent intensity of each lysate was measured by fluorescent spectroscopy. The lysates were also analyzed by ICP-MS, in order to quantify the cellular uptake by measuring the concentration of Au and compare it to the intensity of TAMRA, proportional to the quantity of AuNPs, by fluorescent spectroscopy.

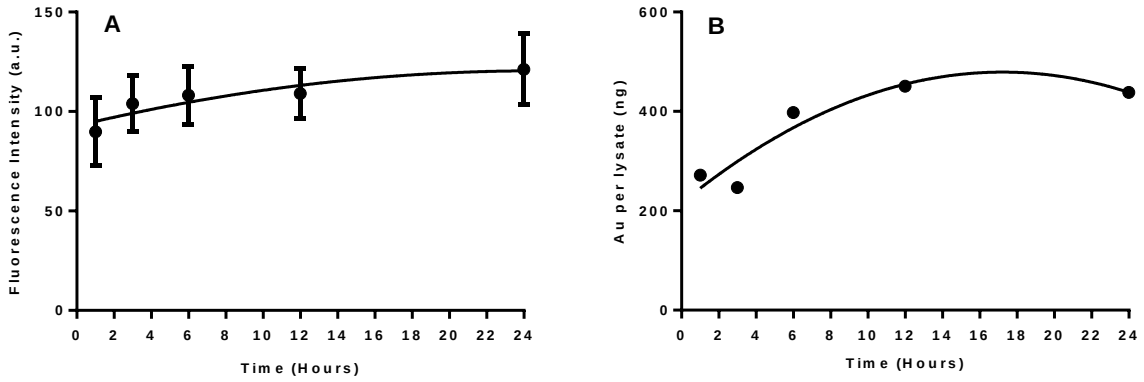

Figure III.5 - Cellular uptake kinetics of AuNPs in A549 cell line. (A) Cellular uptake of 10 nM of AuNPs as function of incubation time quantified by fluorescent spectroscopy. The data is relative to the average of four independent assays each one of them in triplicate and error bars are correspondent to standard deviation (SD). (B) Cellular uptake of 10 nM of AuNPs as function of incubation time quantified by ICP-MS.

Figure III.5 shows the cellular uptake kinetics of AuNPs evaluated by fluorescent spectroscopy (A) and by ICP-MS (B). The uptake of AuNPs significantly increased during the first 6h of incubations, but gradually slowed a reached a plateau after 6h of incubation as represented in Figure III.5A, results that are in agreement with literature reports (Wilhelm et al., 2002; Chithrani et al., 2006). The saturation plateau that is observed is not associated to low quantity or absence of AuNPs in the medium, but probably due to the exocytosis of AuNPs or even due to the distribution of AuNPs between cells following

cell division (Kim et al., 2012). Indeed, the fluorescent data is in agreement with the results obtained by ICP-MS analysis. Although these were not performed in triplicate, a similar kinetics profile was obtained as showed by Figure III.5B. Hence, the similarity between the two analyses ensure that measuring the signal intensity of TAMRA is, in fact, proportional to the quantity of AuNPs present in each lysate.

The cellular uptake kinetics was also evaluated by fluorescent microscopy. However, this technique demonstrated that the AuNPs did not had enough fluorescent intensity capable of distinguish the increment of the AuNPs uptake overtime. This limitation can be to the properties of the fluorescent dye chosen for the attachment to the AuNPs. The emission spectrum of TAMRA dye (572 nm) overlaps with the absorption spectrum of the AuNPs (400 - 700 nm), resulting in a decrease of the fluorescence intensity of TAMRA. This is a known energy transfer mechanism, named Förster Resonance Energy Transfer (FRET) (Park et al., 2012).

Nevertheless, Figure III.6 shows the evaluation of cellular uptake of AuNPs after 24h of incubation by fluorescent microscopy, in order to demonstrate the presence of AuNPs inside the cells.

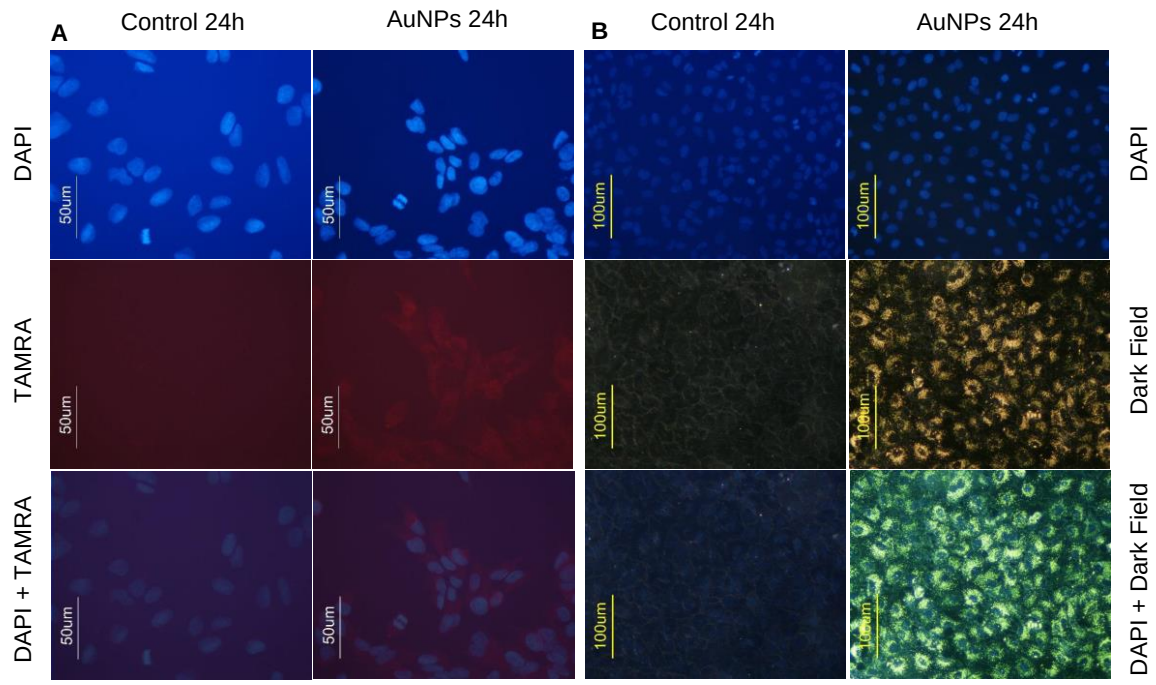

Figure III.6 - Cellular uptake of AuNPs in A549 cell line evaluated by fluorescent microscopy. Images acquired of A549 cells incubated with 10 nM of AuNP@PEG@TAMRA for 24h and the correspondent control (without AuNP incubation. (A) Cellular uptake based on TAMRA fluorescent intensity, (scale bar 50 µm). (B) Cellular uptake based on scattering (dark field) of the gold core, (scale bar 100 µm).

The images were acquired using two different fluorescent filters, a blue one to visualize DAPI stain (imaging of cell nucleus) and a red filter to visualize the TAMRA signaling. Figure III.6A show images of control cells (without AuNPs) and of 24h incubation of AuNPs. The merged image demonstrated the presence of AuNPs around the nucleus, which is indicative of the cellular uptake. Even though the conditions in which fluorescent microscopy was carried do not distinguish the presence of the AuNPs

inside endocytic vesicles or free in the cytosol, previous studies demonstrated that PEG-coated nanoparticles have a higher tendency to appear free within the cytosol. The possible explanation for PEG-coated nanoparticles appear free in the cytosol could be related to PEG high solubility in cell membranes, which can lead to a transmembrane passage of particle from vesicles to cytosol (Brandenberger et al., 2010). The uptake can also be verified in Figure III.6B, where the signaling of TAMRA was replaced by the light dispersion driven by the gold core of this nanoparticles.

Based on the results obtained for the cellular uptake kinetics of the AuNPs, further inhibition studies were performed upon 1, 3, and 6 h of incubation. This time points are set before the saturation plateau of AuNPs cellular uptake. This way, further internalization inhibition results do not be influenced by the exocytosis of AuNPs. Moreover, in this period of time, A549 cells had not yet reached to their doubling time, i.e. the time necessary for double the entire cell population, and the number of cells do not significantly change. Besides, if a primary internalization mechanism is blocked for long periods, cells will attempted to contrary this process, and secondary endocytic pathways will be activated, which can negatively influenced the results from further inhibitions assays.

2.2. MECANISM OF INTERNALIZATION

Different methods have been used to analyze the mechanism of internalization of nanoparticles (Iversen et al., 2011), with one of the most commonly used being the selectively inhibition of the different endocytic pathways through the utilization of pharmacological endocytic inhibitors. A variety of studies have been performed using these endocytic inhibitors in order to assess the internalization mechanism of different types of nanoparticles (Vercauteren et al., 2010; Saha et al., 2013; Rothen-Rutishauser et al., 2014).

To further evaluate the uptake mechanism of the AuNPs prepared, four different endocytic inhibitors, chlorpromazine, filipin, wortmannin and amiloride were used, concerning the three major endocytic pathways, clathrin mediated endocytosis, caveolae mediated endocytosis and macropinocytosis.

So A549 cells were treated with the four endocytic inhibitors in separate, 28.14 µM of chlorpromazine - inhibitor of clathrin mediated endocytosis, 1.53 µM of filipin, inhibitor of caveolae mediated endocytosis, and 300 nM of wortmannin and 1.5 mM of amiloride, inhibitors of macropinocytosis. The cells were treated with these inhibitors for 30 min prior to AuNP incubation, in order to initiate the blockage of each endocytic pathway before the incubation of AuNPs. After this, AuNPs were incubated in presence of each inhibitor to pursue the blockage of each endocytic pathway.

The concentrations of endocytic inhibitors used were based on previous reports, as well as the time of cell treatment with inhibitors before the incubation with AuNPs (Saha et al., 2013; Yang et al., 2013; Rothen-Rutishauser et al., 2014). After incubation, all cellular lysates were measured by fluorescent spectroscopy, in order to determine the TAMRA signal intensity.

The first preliminary experiments regarding the incubation of nanoparticles in presence of amiloride resulted in the aggregation of the AuNPs (Figure III.7), which induced a color change from red (dispersed

AuNPs) to blue (aggregated AuNPs). This change of the solution color is due to a red shift of the SPR band from red to blue, which is induced by the agglomeration of AuNPs, behaving like a larger particle (Baptista et al., 2006).

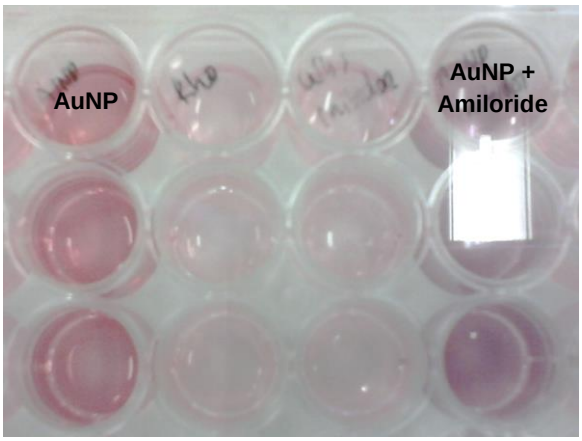

Figure III.7 - Induction of AuNP aggregation by amiloride. In the left: 10 nM AuNPs in culture medium. In the right: 10 nM AuNPs in presence of amiloride in culture medium. A pronounced color change from red to blue indicative of aggregation of AuNPs induced by the presence of amiloride.

The aggregation of AuNPs is known to affect the cellular uptake, sometimes reducing the uptake rate of AuNPs due to a reduced diffusion speed and irregular morphology (Albanese and Chan, 2011). Hence, in the presence of amiloride, the uptake of AuNPs was compromised and the outcome results of cellular uptake in presence of this inhibitor were no longer considered. Moreover, since amiloride and wortmannin are both inhibitors of macropinocytosis, each one responsible for the blockage different mechanisms involved in this endocytic pathway (Ivanov, 2008), only cellular uptake results concerning the inhibition of macropinocytosis with wortmannin were considered.

The effects of endocytic inhibitors on internalization of AuNPs in A549 cell line evaluated by fluorescent spectroscopy are represented in Figure III.8. The cellular uptake of AuNPs without presence of any inhibitor (Control) was set as 100% of cellular uptake, and the percentage of cellular uptake of AuNPs in presence with any inhibitor was determined as function of the control.

Clathrin mediated endocytosis is used by all eukaryotic cells to uptake nutrients and recycle substances, and is known for its role in the selective uptake of molecules. Chlorpromazine, blocking agent of clathrin coated pit formation, decreased the AuNPs cellular uptake in approximately 23.5% after 1h of incubation (Figure III.8A). For the same period of time, filipin, a specific inhibitor of caveolae mediated endocytosis had no significant effect on the cellular uptake of these AuNPs. The same occurred with wortmannin, an inhibitor of micropinocytosis, meaning that the prepared AuNPs seem to be uptake by cells manly through clathrin mediated endocytosis.

The effect of chlorpromazine on the cellular uptake of these AuNPs may be due to the amphipathic nature of this inhibitor. This property allows chlorpromazine to rapidly incorporate into the plasma

membrane increasing lipid fluidity, which can lead to a decrease on AuNP internalization (Gratton et al., 2008; Ivanov, 2008).

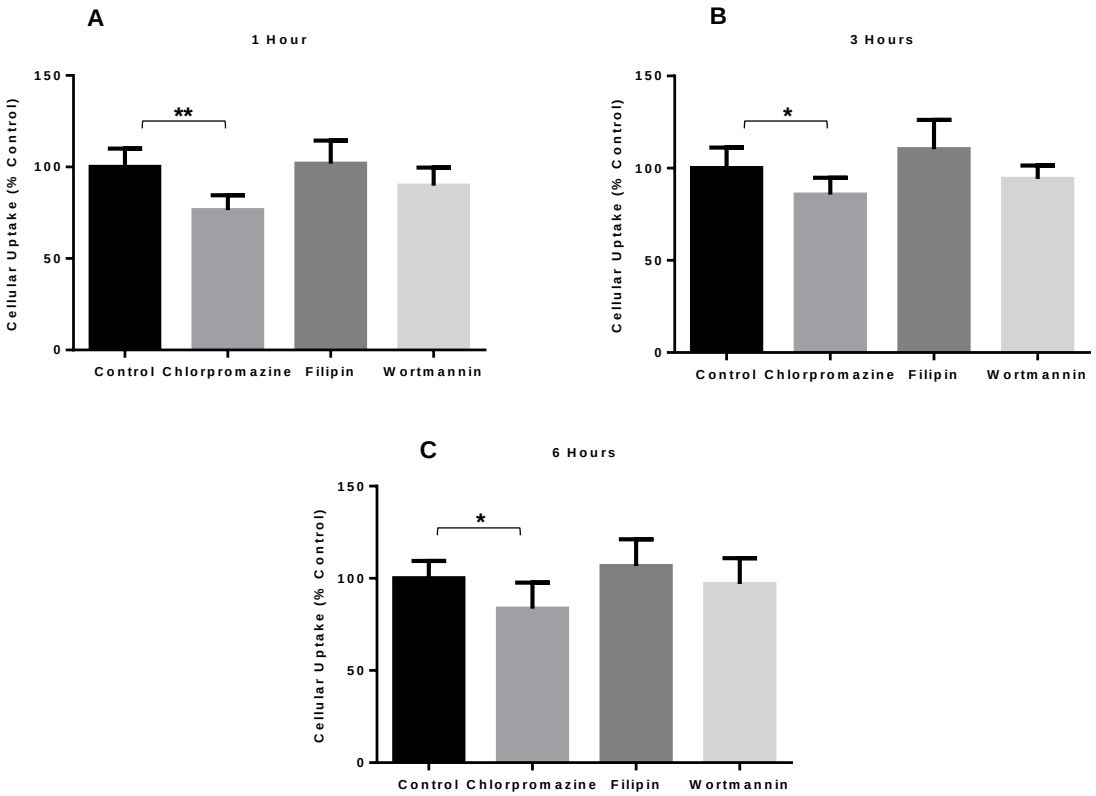

Figure III.8 - Effects of endocytic inhibitors on internalization of AuNPs in A549 cell line evaluated by fluorescent spectroscopy. Internalization of 10 nM of AuNP@PEG@TAMRA. Cells were treated with 28.14 µM of chlorpromazine, 1.53 µM of filipin and 300 nM of wortmannin for 30 min before incubation with 10 nM of AuNPs for 1h (A), 3h (B) and 6h (C), all cellular lysates were measured by fluorescent spectroscopy. The fluorescent intensity of the cellular uptake of AuNP without inhibitors (control) was set as 100%. The data is relative to the average of four independent assays each of one in triplicate and error bars are correspondent to SD (* $P < 0.05$; ** $P < 0.01$).

However, the effect of chlorpromazine on the internalization of AuNPs appears to be dependent on the incubation time, since its effect seems to diminish, and after 3h of incubation, the cellular uptake only decreased 16.5% in presence of this inhibitor, and after 6h, the inhibition effect of chlorpromazine was decreased to 14.4%. As for the effect of wortmannin or filipin on the cellular uptake of the AuNPs (Figure III.8B and Figure III.8C), the increase in incubation time had no impact in the internalization of AuNPs.

Although chlorpromazine was present for all incubation times, the decrease in the inhibitory effect of this drug with the increase of the incubation time could be related to the activation of other endocytic pathway routes induced by blocking the clathrin-mediated endocytosis (Connor et al., 2005; Harush-Frenkel et al., 2007). Moreover, inhibition of the clathrin coated pits upregulates other internalization pathways, which with the increase of the incubation time can induce the recovery of cellular uptake, explaining the results of chlorpromazine at 3h and 6h of incubation (Ivanov, 2008; Vercauteren et al., 2010).

Uptake kinetics of clathrin-mediated endocytosis is much faster than the other endocytic pathways (Rejman et al., 2005). Based on this, the fact that chlorpromazine caused higher effect for 1h of incubation, meaning that this AuNPs might undergo internalization by clathrin mediated endocytosis that is in agreement with the fast kinetics results obtaining for the cellular uptake of the AuNPs.

Once, a significant cellular uptake inhibition, evaluated by fluorescent spectroscopy, was achieved after 1 hour of incubation, the samples regarding this experimental condition were also evaluated by ICP-MS (Figure III.9).

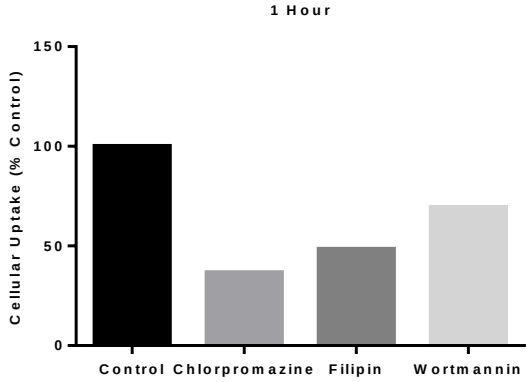

Figure III.9 - Effects of endocytic inhibitors on internalization of AuNPs in A549 cell line evaluated by ICP-MS. Internalization of 10 nM of AuNP@PEG@TAMRA. Cells were treated with 28.14 µM of chlorpromazine, 1.53 µM of filipin and 300 nM of wortmannin for 30 min before incubation with 10 nM of AuNPs for 1h all cellular lysates were measured by ICP-MS. The quantity of gold present on the cellular uptake of AuNP without inhibitors (control) was set as 100%.

The uptake inhibition data represented on Figure III.9 is relative to a single measurement. The results are significantly different from the ones obtained by fluorescent spectroscopy, however a similar tendency is attained. Chlorpromazine continues to have the higher inhibition effect on the internalization of AuNPs, c.a. 63% of inhibition, followed by filipin (52% of inhibition) and wortmannin (31% of inhibition). The major differences obtained between the two methods used to evaluate the cellular uptake inhibition could be due to a small number of sample replicates measured by ICP-MS.

Although the results obtained by ICP-MS are merely indicative, clathrin-mediated endocytosis (inhibited by chlorpromazine) seems to be the primary internalization mechanism of this AuNPs. However, as evidenced by results obtained by fluorescent spectroscopy, other endocytic mechanisms appears to be involved on this AuNPs cellular uptake, most likely caveolae-mediated endocytosis, which is blocked by filipin.

To better understand all the mechanism involved on the uptake of this AuNPs, A549 cells were treated with different combination sets of the three endocytic inhibitors previously used, wortmannin + filipin, wortmannin + chlorpromazine, filipin + chlorpromazine and wortmannin + filipin + chlorpromazine.

The effects of combination of endocytic inhibitors on internalization of AuNPs in A549 cell line evaluated by fluorescent spectroscopy are represented in Figure III.10. The cellular uptake of AuNPs without

presence of any inhibitor (Control) was set as 100% of cellular uptake, and the percentage of cellular uptake of AuNPs in presence with any inhibitor was set as function of the control.

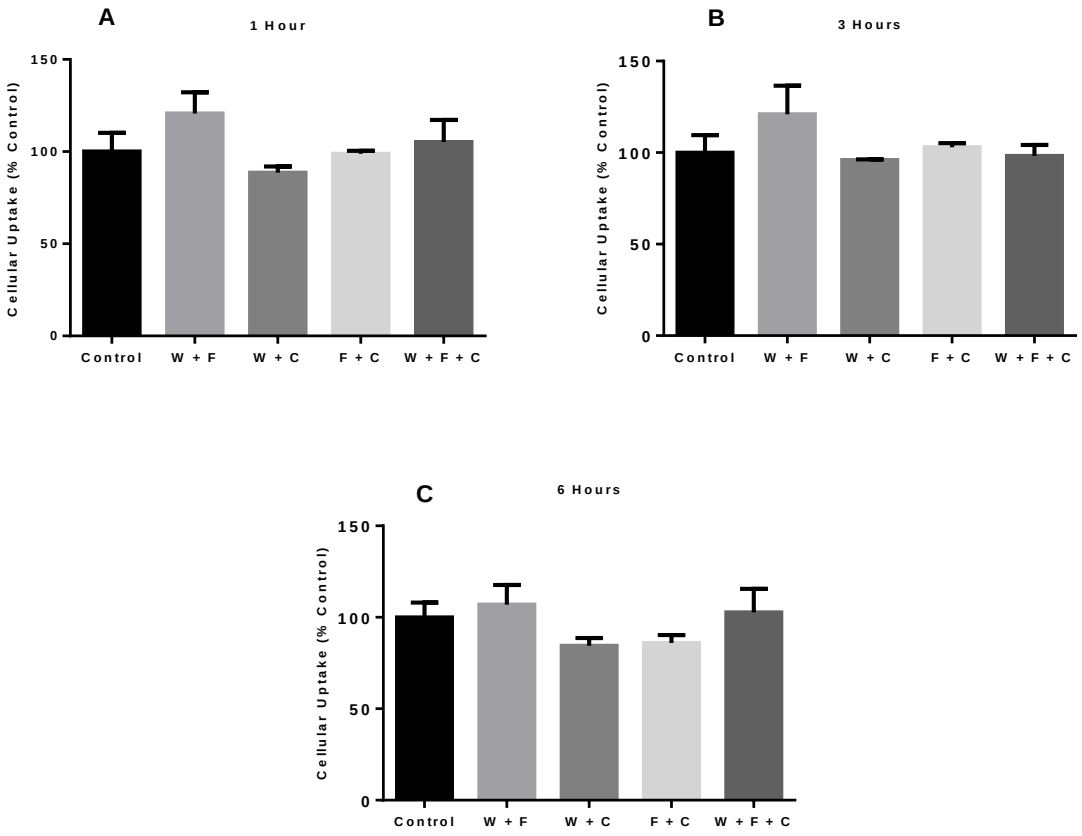

Figure III.10 - Effects of combination of endocytic inhibitors on internalization of AuNPs in A549 cell line evaluated by fluorescent spectroscopy. Internalization of 10 nM of AuNP@PEG@TAMRA. Cells were treated with combined sets of 28.14 µM of chlorpromazine (C), 1.53 µM of filipin (F) and 300 nM of wortmannin (W) for 30 min before incubation with 10 nM of AuNPs for 1h (A), 3h (B) and 6h (C), all cellular lysates were measured by fluorescent spectroscopy The fluorescent intensity of the cellular uptake of AuNP without inhibitors (control) was set as 100%. The data is relative to the average of one independent assays in triplicate and error bars are correspondent to SD.

The combination of wortmannin and filipin had no effect on the cellular uptake during all incubation times, similarly to what was observed when these inhibitors were used by their own. The same was observed for the combination of all three inhibitors. Even though chlorpromazine was present in the sample test, no effect on the uptake has been detected. On the other hand, the combination of chlorpromazine with wortmannin or filipin resulted in decreased cellular uptake, but always inferior to the effect of chlorpromazine alone (10 - 12% of inhibition).

Additionally, the samples related to the effect of combination of endocytic inhibitors on AuNPs cellular uptake after 1 hour of incubation were also evaluated by ICP-MS (Figure III.11).

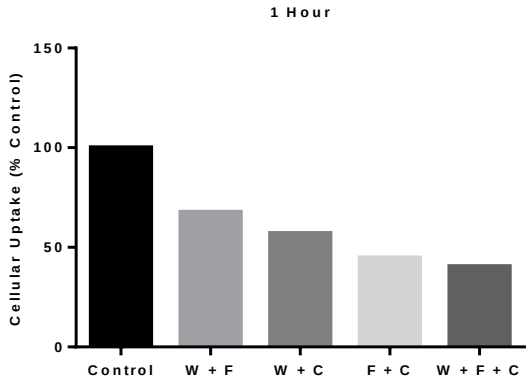

Figure III.11 - Effects of combination of endocytic inhibitors on internalization of AuNPs in A549 cell line evaluated by ICP-MS. Internalization of 10 nM of AuNP@PEG@TAMRA. Cells were treated with combined sets of 28.14 µM of chlorpromazine (C), 1.53 µM of filipin (F) and 300 nM of wortmannin (W) for 30 min before incubation with 10 nM of AuNPs for 1h, all cellular lysates were measured by ICP-MS. The quantity of gold present on the cellular uptake of AuNP without inhibitors (control) was set as 100%.

The uptake inhibition data represented on Figure III.11 is relative to a single measurement. Once again, the results are significantly different from the ones obtained by fluorescent spectroscopy. The combination of chlorpromazine with wortmannin or filipin resulted in 43% and 55% of inhibition, respectively. The combination of wortmannin and filipin resulted in 32% of inhibition and the combination of all inhibitors resulted in 60% of inhibition. Although all combinations of inhibitors had resulted in inhibition of cellular uptake of AuNPs, the presence of chlorpromazine results always in higher inhibition effects, when compared with the inhibition effect induced by the combination with wortmannin and filipin. As evidenced by the results obtained by fluorescent spectroscopy, the combination of endocytic inhibitors resulted always on inferior inhibition effects when compared with the effect of chlorpromazine alone (c.a. 63% of inhibition).

Based on the results, it can be assumed that these AuNPs were primarily uptake by clathrin mediated endocytosis. Further studies with different analytical techniques, such as intracellular co-localization of AuNPs by confocal microscopy should be address in order to fully understand the mechanism of internalization. Although the effect of these inhibitors on the cellular uptake of AuNPs had been also evaluated by fluorescent microscopy, the TAMRA signaling was not adequate for correct evaluation, as mentioned before.

However these results are in concordance in previous studies in literature. Various reports revealed different types of nanoparticles that seem to be internalized by clathrin mediated endocytosis (M. Huang et al., 2002; Harush-Frenkel et al., 2007; Nan et al., 2008; Vasir and Labhasetwar, 2008). The reduced size (up to 150 nm) is the main common characteristic of this different nanoparticles, maybe because clathrin coated pits are rigid structures forming an endosomal invagination with a maximum diameter of 100 - 150 nm (Dausend et al., 2008).

3. CELL VIABILITY OF GOLD NANOPARTICLES AND ENDOCYTIC INHIBITORS

To validate the previously reported results, it was imperative to evaluate the effect of the prepared AuNPs and endocytic inhibitors on the cell viability. The MTS assay was used and in this test, MTS is reduced to formazan by metabolically active cells. The amount of formazan produced, measured spectroscopically at 490 nm, is proportional to the amount of viable cells (metabolically active).

First, cell viability was investigated after exposure to a range of concentrations of AuNPs for 24 hours. After the period of incubation, AuNPs were replaced by fresh culture medium and the MTS assay was performed after 24h. The percentage of cell viability obtained for A549 cell line is represented in Figure III.12.

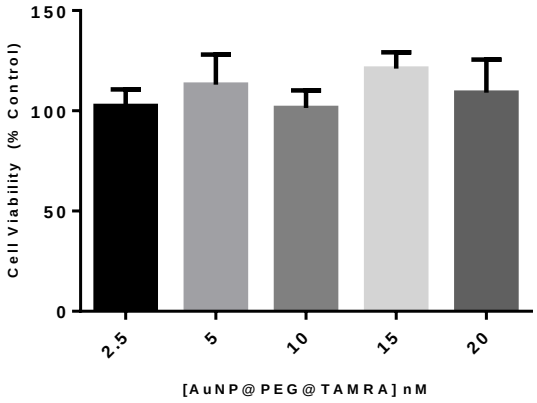

Figure III.12 - Cell viability in A549 cell after exposure to AuNPs obtained by MTS assay. A range of concentration of AuNPs (2.5 - 20 nM) was incubated for 24h. All results of cell viability were function of the control (without AuNPs), which was set to 100%. Data is relative to the average of three independent assays and error bars are correspondent to SD.

There were no significant changes of cell viability for all the concentration of AuNPs tested upon 24 hours of incubation.

Next, it was necessary to evaluate the cell viability after treating A549 cells with the endocytic inhibitors in presence and absence of AuNPs. So, A549 cells were treated with endocytic inhibitors for 30 min, and then incubated with AuNPs in presence of inhibitors for 6h. After the period of incubation, AuNPs were replaced by fresh culture medium and the MTS assay was performed after 24h. The percentage of cell viability obtained for A549 cell line is represented in Figure III.13. Once again, the endocytic inhibitors and AuNPs in presence of inhibitors had no significant effect on cell viability up to 6h, for these experimental conditions.

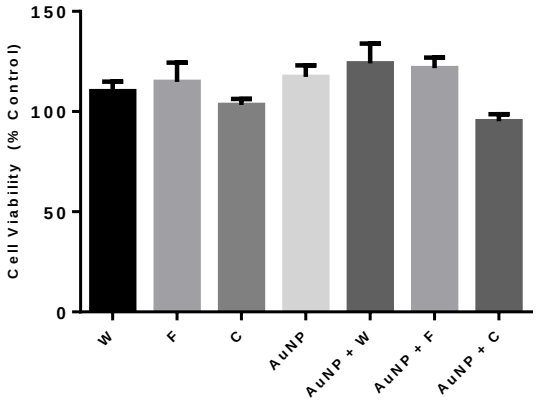

Figure III.13 **- Cell viability in A549 cell after exposure to AuNPs in presence and absence of endocytic inhibitors obtained by MTS assay.** A549 cells were treated with chlorpromazine (C), filipin (F) and wortmannin (W) for 30 min prior to the incubation of 10 nM of AuNPs for 6h. All results of cell viability were function of the control (without AuNPs and inhibitors), which was set to 100%. The data is relative to the average of three independent assays and error bars are correspondent to SD.

Another two assays were performed to evaluate the cell viability in presence of these endocytic inhibitors, a cell count by trypan blue staining and a cell count by nucleus staining. These two assays were also performed in order to guarantee that in all the experiments regarding inhibition of cellular uptake, the number of viable cells of each condition was similar, so as to allow direct comparison of data.

The trypan blue assay is based on a differential staining of non-viable cells in opposite to viable ones. Trypan blue is a blue dye that can trespass the plasma membrane of non-viable cells, in which the plasma membrane is more permeable. To evaluate cell viability by this assay, A549 cells were treated with chlorpromazine, wortmannin and filipin for 30 min, and then AuNP were incubated in presence of the same inhibitors. After the period of incubation, the cells were detached and the number of cells was determined - Figure III.14. The number of cells correspondent to control (without inhibitors and AuNP) was set to 100% of cell viability and the cell viability of the other conditions was function of the control. The endocytic inhibitors and AuNPs in presence of inhibitors had no significant effect on cell viability evaluated by cell count by trypan blue, under these experimental conditions, as verified also by the MTS assay.

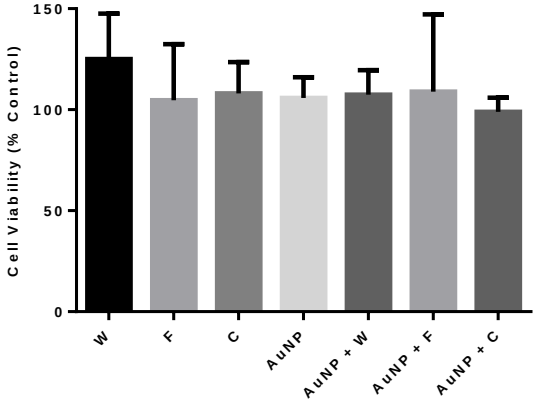

Figure III.14 - Cell viability in A549 cell after exposure to AuNPs in presence and absence of endocytic inhibitors obtained by cell count by trypan blue. A549 cells were treated with chlorpromazine (C), filipin (F) and wortmannin (W) for 30 min prior to the incubation of 10 nM of AuNPs for 6h. All results of cell viability were function of the control (without AuNPs and inhibitors), which was set to 100%. The data is relative to the average of three independent assays and error bars are correspondent to SD.

Finally, cell viability was assessed by cell count by nucleus staining with DAPI. A549 cells were treated with chlorpromazine, wortmannin and filipin for 30 min, and then AuNP were incubated in presence of the same inhibitors. After the incubation period, cells were fixed and the nucleus were staining with DAPI, a dye that has high affinity to nucleic acids, allowing the visualization of cellular nucleus by fluorescent microscopy. The number of nucleus with normal morphology was counted and the number of viable cells was determined.

The percentage of cell viability evaluated by cell count by nucleus staining is represented in Figure III.15. The number of cells correspondent to control (without inhibitors and AuNP) was set to 100% of cell viability and the cell viability of the other conditions was function of the control.

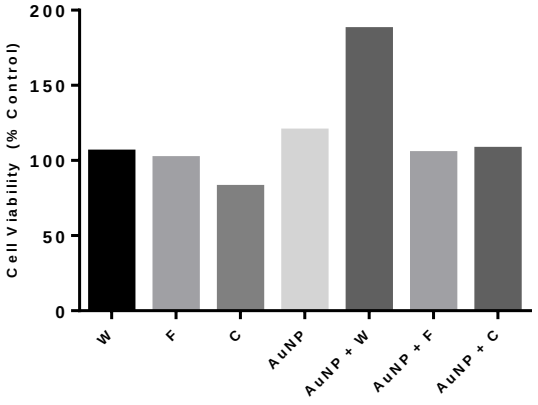

Figure III.15 - Cell viability in A549 cell after exposure to AuNPs in presence and absence of endocytic inhibitors obtained by cell count by nucleus staining. A549 cells were treated with chlorpromazine (C), filipin (F) and wortmannin (W) for 30 min prior to the incubation of 10 nM of AuNPs for 6h. All results of cell viability were function of the control (without AuNPs and inhibitors), which was set to 100%.

Once again, the endocytic inhibitors and AuNPs in presence of inhibitors had no significant effect on cell viability up to 6h of incubation, under these experimental conditions. Only AuNPs in presence of wortmannin induced an increase on the cell viability, however this result most likely is due to an experimental mistake that could not be detected because the experience was only performed once. Therefore, it can be assumed that the decreased on the cellular uptake induced by chlorpromazine is only due to the activity of the pharmacological inhibitor and not due to a decrease in cell viability. Besides, the data outcome by cell count by trypan blue staining and cell count by nucleus staining suggest that number of cells of each condition remains similar, meaning that the results regarding inhibition of cellular uptake can be comparable.

IV. CONCLUSION AND FUTURE PRESPECTIVES

The present work addressed the study of cellular uptake kinetics and internalization mechanism of 14 nm spherical AuNPs by fluorescent spectroscopy and ICP-MS in A549 cell line. Additionally, the cellular uptake was studied by fluorescent microscopy to confirm the presence of AuNPs in the intracellular environment.

Spherical AuNPs were successfully prepared by the citrate reduction method with an average diameter of 14 nm determined by TEM and a hydrodynamic diameter of 18 nm acquired by DLS. The colloidal solution was also characterized by UV-visible spectroscopy, obtaining a maximum and symmetric SPR peak at 518 nm, typical of a monodisperse solution. The AuNPs were functionalized with PEG in order to increase their stability and biocompatibility and also to allow further functionalization with TAMRA (fluorescent dye) by EDC/NHS coupling reaction. The prepared TAMRA labeled AuNPs presented a finally hydrodynamic diameter of 23 nm attained by DLS.

Fluorescent spectroscopy revealed that the prepared AuNPs had rapid cellular uptake kinetics (presence of AuNPs inside the cell after 1 hour of incubation), reaching a saturation point after 6 hours of incubation. This result was also confirmed by ICP-MS, revealing a correlation between TAMRA signaling present in the cellular lysates obtained by fluorescent spectroscopy and the amount of gold present in the same cellular lysates determined by ICP-MS.

Using three different endocytic inhibitors, efficient cellular uptake inhibition of AuNPs was only achieved with 28.14 µM of chlorpromazine, presenting a confidence interval of 99% (*p value* < 0.01) for 1 hour of incubation and 95% (*p value* < 0.05) for 3 and 6 hours of incubation. The others inhibitors (wortmannin and filipin) and combination of inhibitors did not significantly affected the AuNP uptake (Table IV.1).

Table IV.1 - Summary of cellular uptake inhibition of AuNPs obtained by fluorescent spectroscopy.

Inhibitor	Endocytic pathway	1 hour	3 hours	6 hours
Wortmannin	Macropinocytosis	Ø	Ø	Ø
Filipin	Caveolae-mediated	Ø	Ø	Ø
Chlorpromazine	Clathrin-mediated	+++	++	++
Wortmannin + Filipin	Macropinocytosis + Caveolae-mediated	Ø	Ø	Ø
Wortmannin + Chlorpromazine	Macropinocytosis + Clathrin-mediated	+	+	+
Filipin + Chlorpromazine	Caveolae-mediated + Clathrin-mediated	Ø	+	+
Wortmannin + Filipin + Chlorpromazine	Macropinocytosis + Caveolae-mediated + Clathrin-mediated	Ø	Ø	Ø

(Ø): no significant inhibition effect; (+): inhibition up to 13 %; (++): inhibition between 13 and 20 %; (+++): inhibition superior to 20 %.

The fact that in this experimental condition chlorpromazine only inhibited the cellular uptake in about 23.5% may suggest the these AuNPs were manly taken up by clathrin-mediated endocytosis, but still other endocytic mechanisms could be involved.

Furthermore, the cell viability assay demonstrated that the prepared AuNPs and the three endocytic inhibitors used did not induced relevant alterations in the cell viability of A549 cell line, under the tested experimental conditions.

Data here presented seem to support that the prepared AuNPs are mainly internalized by clathrin-mediated endocytosis. Nevertheless, results still reflect a preliminary study and several experimental conditions should be assessed to better understand the mechanism of internalization:

- It is important fully understand the role of clathrin-mediated endocytosis on the internalization of these AuNPs. In this regard, additional inhibition assays should be performed with increasing concentrations of chlorpromazine to maximize the effect of this inhibitor without compromise cell viability. Furthermore, supplementary inhibition assays with potassium depletion, reported to specifically inhibit clathrin-mediated endocytosis, should be addressed. If inhibition of cellular uptake is verified applying the potassium depletion, complementary inhibition studies should be performed, combining potassium depletion and chlorpromazine;
- Several reports highlighted the problem related to the unspecificity of endocytic inhibitors for a single internalization pathway. On this basis, complementary approaches should be implemented to evaluate the internalization mechanism of these AuNPs, including co-localization of intracellular AuNPs by confocal microscopy. This approaches allows the labeling of different intracellular organelles, such as caveolae (caveolae-mediated endocytosis), clathrin-coated pits (clathrin-mediated endocytosis), early and late endosomes, and lysosomes.
- To completely understand the interaction of the AuNPs used currently in our laboratory with living cells, additional assays should be achieved to evaluate the internalization mechanism in function of surface chemistry (charge and targeting agents) and in function of cell type. These studies will allow the design and optimization of AuNPs for therapeutic approaches. Since nanoparticles internalized by caveolae-mediated endocytosis are prone to escape lysosomal degradation, releasing its content directly to the cytosol, new AuNPs should be designed to target the caveolae-mediated endocytosis. For this this purpose, AuNPs surface can be functionalized with targets to caveolae for example with the monoclonal antibody that targets the aminopeptidase P (AAP) which binds to caveolae enriched with APP (Oh et al., 2007). Another targeting molecule is cyclic RGD peptide. This peptide binds to an integrin receptor located in caveolae (Oba et al., 2008).

Although this studies offer valuable insights into gold nanoparticles interaction with living cell and biological systems, several other issues should be address in future researches, including exocytosis patterns and long-term studies regarding gold nanoparticles cytotoxicity. However, the understanding the underling mechanisms of gold nanoparticles - cell interface allow the possibility to design and optimize new nanotechnology approaches from basic research to clinical application.

V. REFERENCES

Albanese, A., & Chan, W. C. W. (2011). Effect of Gold Nanoparticle Aggregation on Cell Uptake and Toxicity. *ACS Nano*, *5*(7), 5478–5489.

Balasubramanian, N., Scott, D. W., Castle, J. D., Casanova, J. E., & Schwartz, M. A. (2009). Arf6 and microtubules in adhesion-dependent trafficking of lipid rafts. *Cell*, *9*(12), 1381–1391.

Baptista, P., Doria, G., Henriques, D., Pereira, E., & Franco, R. (2005). Colorimetric detection of eukaryotic gene expression with DNA-derivatized gold nanoparticles. *Journal of Biotechnology*, *119*(2), 111–7.

Baptista, P. V, Koziol-Montewka, M., Paluch-Oles, J., Doria, G., & Franco, R. (2006). Gold-nanoparticle-probe-based assay for rapid and direct detection of Mycobacterium tuberculosis DNA in clinical samples. *Clinical Chemistry*, *52*(7), 1433–4.

Baptista, P. V, Pereira, E., Eaton, P., Doria, G., Miranda, A., Gomes, I., … Franco, R. (2008). Gold nanoparticles for the development of clinical diagnosis methods. *Analytical and Bioanalytical Chemistry*, *391*(3), 943–950.

Bhattacharyya, S., Kudgus, R. A., Bhattacharya, R., & Mukherjee, P. (2011). Inorganic nanoparticles in cancer therapy. *Pharmaceutical Research*, *28*(2), 237–259.

Boisselier, E., & Astruc, D. (2009). Gold nanoparticles in nanomedicine: preparations, imaging, diagnostics, therapies and toxicity. *Chemical Society Reviews*, *38*(6), 1759–1782.

Brandenberger, C., Mühlfeld, C., Ali, Z., Lenz, A. G., Schmid, O., Parak, W. J., … Rothen-Rutishauser, B. (2010). Quantitative evaluation of cellular uptake and trafficking of plain and polyethylene glycol-coated gold nanoparticles. *Small*, *6*(15), 1669–1678.

Cabral, R. M., & Baptista, P. V. (2014). Anti-cancer precision theranostics: a focus on multifunctional gold nanoparticles. *Expert Review of Molecular Diagnostics*, *14*(8), 1041–1052.

Cai, W., Gao, T., Hong, H., & Sun, J. (2008). Applications of gold nanoparticles in cancer nanotechnology. *Nanotechnology, Science and Applications*, *1*, 17–32.

Cai, W., Shin, D. W., Chen, K., Gheysens, O., Cao, Q., Wang, S. X., … Chen, X. (2006). Peptide-labeled near-infrared quantum dots for imaging tumor vasculature in living subjects. *Nano Letters*, *6*(4), 669–676.

Canton, I., & Battaglia, G. (2012). Endocytosis at the nanoscale. *Chemical Society Reviews*, *41*, 2718–2739.

Chithrani, B. D., & Chan, W. C. W. (2007). Elucidating the mechanism of cellular uptake and removal of protein-coated gold nanoparticles of different sizes and shapes. *Nano Letters*, *7*(6), 1542–1550.

Chithrani, B. D., Ghazani, A. a., & Chan, W. C. W. (2006). Determining the size and shape dependence of gold nanoparticle uptake into mammalian cells. *Nano Letters*, *6*(4), 662–668.

Chithrani, D. B. (2010). Intracellular uptake, transport, and processing of gold nanostructures. *Molecular Membrane Biology*, *27*(7), 299–311.

Cho, E. C., Xie, J., Wurm, P. a., & Xia, Y. (2009). Understanding the role of surface charges in cellular adsorption versus internalization by selectively removing gold nanoparticles on the cell surface with a I 2/KI etchant. *Nano Letters*, *9*(3), 1080–1084.

Conde, J., Ambrosone, A., Sanz, V., Hernandez, Y., Marchesano, V., Tian, F., de la Fuente, J. M. (2012). Design of multifunctional gold nanoparticles for *in vitro* and *in vivo* gene silencing. *ACS Nano*, (9), 8316–8324.

Conde, J., Dias, J. T., Grazú, V., Moros, M., Baptista, P. V, & de la Fuente, J. M. (2014). Revisiting 30 years of biofunctionalization and surface chemistry of inorganic nanoparticles for nanomedicine. *Frontiers in Chemistry*, *2*, 1–27.

Conde, J., Tian, F., Hernández, Y., Bao, C., Cui, D., Janssen, K. P., de la Fuente, J. M. (2013). *In vivo* tumor targeting via nanoparticle-mediated therapeutic siRNA coupled to inflammatory response in lung cancer mouse models. *Biomaterials*, *34*(31), 7744–7753.

Connor, E. E., Mwamuka, J., Gole, A., Murphy, C. J., & Wyatt, M. D. (2005). Gold nanoparticles are taken up by human cells but do not cause acute cytotoxicity. *Small*, *1*(3), 325–327.

Daniel, M., & Astruc, D. (2004). Gold Nanoparticles : Assembly , Supramolecular Chemistry , Quantum-Size-Related Properties , and Applications toward Biology , Catalysis , and Nanotechnology Gold Nanoparticles : Assembly , Supramolecular Chemistry , Quantum-Size-Related Properties , and. *Chemical Reviews*, *104*(1), 293–346.

Dausend, J., Musyanovych, A., Dass, M., Walther, P., Schrezenmeier, H., Landfester, K., & Mailänder, V. (2008). Uptake mechanism of oppositely charged fluorescent nanoparticles in Hela cells. *Macromolecular Bioscience*, *8*(12), 1135–1143.

DeLong, R. K., Reynolds, C. M., Malcolm, Y., Schaeffer, A., Severs, T., & Wanekaya, A. (2010). Functionalized gold nanoparticles for the binding, stabilization, and delivery of therapeutic DNA, RNA, and other biological macromolecules. *Nanotechnology, Science and Applications*, *3*(1), 53–63.

Dreaden, E. C., Alkilany, A. M., Huang, X., Murphy, C. J., & El-Sayed, M. a. (2012). The golden age: gold nanoparticles for biomedicine. *Chemical Society Reviews*, *41*(7), 2740–2779.

Elsaesser, A., Taylor, A., de Yanés, G. S., McKerr, G., Kim, E.-M., O'Hare, E., & Howard, C. V. (2010). Quantification of nanoparticle uptake by cells using microscopical and analytical techniques. *Nanomedicine*, *5*(9), 1447–1457.

Eustis, S., & el-Sayed, M. a. (2006). Why gold nanoparticles are more precious than pretty gold: noble metal surface plasmon resonance and its enhancement of the radiative and nonradiative properties of nanocrystals of different shapes. *Chemical Society Reviews*, *35*(3), 209–217.

Grabarek, Z., & Gergely, J. (1990). Zero-length crosslinking procedure with the use of active esters. *Analytical Biochemistry*, *185*(1), 131–135.

Gratton, S. E. a, Ropp, P. a, Pohlhaus, P. D., Luft, J. C., Madden, V. J., Napier, M. E., & DeSimone, J. M. (2008). The effect of particle design on cellular internalization pathways. *Proceedings of the National Academy of Sciences of the United States of America*, *105*(33), 11613–11618.

Harush-Frenkel, O., Debotton, N., Benita, S., & Altschuler, Y. (2007). Targeting of nanoparticles to the clathrin-mediated endocytic pathway. *Biochemical and Biophysical Research Communications*, *353*(1), 26–32.

Heo, D. N., Yang, D. H., Moon, H. J., Lee, J. B., Bae, M. S., Lee, S. C., … Kwon, I. K. (2012). Gold nanoparticles surface-functionalized with paclitaxel drug and biotin receptor as theranostic agents for cancer therapy. *Biomaterials*, *33*(3), 856–866.

Hu, M., Chen, J., Li, Z.-Y., Au, L., Hartland, G. V, Li, X., … Xia, Y. (2006). Gold nanostructures: engineering their plasmonic properties for biomedical applications. *Chemical Society Reviews*, *35*(11), 1084–94.

Huang, M., Ma, Z., Khor, E., & Lim, L. Y. (2002). Uptake of FITC-chitosan nanoparticles by A549 cells. *Pharmaceutical Research*, *19*(10), 1488–1494.

Huang, X., Jain, P. K., El-Sayed, I. H., & El-Sayed, M. a. (2007). Gold nanoparticles: interesting optical properties and recent applications in cancer diagnostics and therapy. *Nanomedicine*, *2*(5), 681–93.

Iris Biotech GMBH, Reagents. http://www.iris-biotech.de/ (accessed in August, 2015).

Ivanov, A. I. (2008). *Endocytosis and Exocytosis*. (A. I. Ivanov, Ed.)*Methods in Molecular Biology* (1st ed., Vol. 440). Totowa, NJ: Humana Press.

Iversen, T. G., Skotland, T., & Sandvig, K. (2011). Endocytosis and intracellular transport of nanoparticles: Present knowledge and need for future studies. *Nano Today*, *6*(2), 176–185.

Jain, K. K. (2008). Nanomedicine: application of nanobiotechnology in medical practice. *Medical Principles and Practice : International Journal of the Kuwait University, Health Science Centre*, *17*(2), 89–101.

Jain, P. K., Lee, K. S., El-Sayed, I. H., & El-Sayed, M. a. (2006). Calculated absorption and scattering properties of gold nanoparticles of different size, shape, and composition: applications in biological imaging and biomedicine. *The Journal of Physical Chemistry. B*, *110*(14), 7238–7248.

Joh, D. Y., Kao, G. D., Murty, S., Stangl, M., Sun, L., Al Zaki, A., Dorsey, J. F. (2013). Theranostic gold nanoparticles modified for durable systemic circulation effectively and safely enhance the radiation therapy of human sarcoma cells and tumors. *Translational Oncology*, *6*(6), 722–31.

Jokerst, J. V, Lobovkina, T., Zare, R. N., & Gambhir, S. S. (2012). Nanoparticle PEGylation for imaging and therapy. *Nanomedicine*, *6*(4), 715–728.

Kim, D., Jeong, Y. Y., & Jon, S. (2010). A drug-loaded aptamer-gold nanoparticle bioconjugate for combined CT imaging and therapy of prostate cancer. *ACS Nano*, *4*(7), 3689–3696.

Kim, J. A., Aberg, C., Salvati, A., & Dawson, K. A. (2012). Role of cell cycle on the cellular uptake and dilution of nanoparticles in a cell population. *Nature Nanotechnology*, *7*, 62–68.

Lammers, T., Aime, S., Hennink, W. E., Storm, G., & Kiessling, F. (2011). Theranostic nanomedicine. *Accounts of Chemical Research*, *44*(10), 1029–1038.

Lee, P. C., & Meisel, D. (1982). Adsorption and surface-enhanced Raman of dyes on silver and gold sols. *Journal of Physical Chemical*, *86*(17), 3391–3395.

Liu, Z., Cai, W., He, L., Nakayama, N., Chen, K., Sun, X., … Dai, H. (2007). *In vivo* biodistribution and highly efficient tumour targeting of carbon nanotubes in mice. *Nature Nanotechnology*, *2*, 47–52.

Mahmoudi, M., Serpooshan, V., & Laurent, S. (2011). Engineered nanoparticles for biomolecular imaging. *Nanoscale*, *3*(8), 3007–3026.

Mayor, S., & Pagano, R. E. (2007). Pathways of clathrin-independent endocytosis. *Nature Reviews. Molecular Cell Biology*, *8*(8), 603–612.

Nan, A., Bai, X., Son, S. J., Lee, S. B., & Ghandehari, H. (2008). Cellular uptake and cytotoxicity of silica nanotubes. *Nano Letters*, *8*(8), 2150–2154.

Oba, M., Aoyagi, K., Miyata, K., Matsumoto, Y., Itaka, K., Nishiyama, N., Kataoka, K. (2008). Polyplex micelles with cyclic RGD peptide ligands and disulfide cross-links directing to the enhanced transfection via controlled intracellular trafficking. *Molecular Pharmaceutics*, *5*(6), 1080–1092.

Oh, N., & Park, J.-H. (2014). Endocytosis and exocytosis of nanoparticles in mammalian cells. *International Journal of Nanomedicine*, *9*, 51–63.

Oh, P., Borgström, P., Witkiewicz, H., Li, Y., Borgström, B. J., Chrastina, A., Schnitzer, J. E. (2007). Live dynamic imaging of caveolae pumping targeted antibody rapidly and specifically across endothelium in the lung. *Nature Biotechnology*, *25*(3), 327–337.

Owens III, D. E., & Peppas, N. a. (2006). Opsonization, biodistribution, and pharmacokinetics of polymeric nanoparticles. *International Journal of Pharmaceutics*, *307*(1), 93–102.

Park, J. W., Benz, C. C., & Martin, F. J. (2004). Future directions of liposome- and immunoliposome-based cancer therapeutics. *Seminars in Oncology*, *31*(13), 196–205.

Park, S. Y., Lee, S. M., Kim, G. B., & Kim, Y. P. (2012). Gold nanoparticle-based fluorescence quenching via metal coordination for assaying protease activity. *Gold Bulletin*, *45*(4), 213–219.

Rejman, J., Bragonzi, A., & Conese, M. (2005). Role of clathrin- and caveolae-mediated endocytosis in gene transfer mediated by lipo- and polyplexes. *Molecular Therapy*, *12*(3), 468–474.

Rothen-Rutishauser, B., Kuhn, D. a, Ali, Z., Gasser, M., Amin, F., Parak, W. J., … Brandenberger, C. (2014). Quantification of gold nanoparticle cell uptake under controlled biological conditions and adequate resolution. *Nanomedicine*, *9*(5), 607–21.

Saha, K., Kim, S. T., Yan, B., Miranda, O. R., Alfonso, F. S., Shlosman, D., & Rotello, V. M. (2013). Surface functionality of nanoparticles determines cellular uptake mechanisms in mammalian cells. *Small*, *9*(2), 300–305.

Sahay, G., Alakhova, D. Y., & Kabanov, A. V. (2010). Endocytosis of nanomedicines. *Journal of Controlled Release*, *145*(3), 182–195.

Salomon, J. J., & Ehrhardt, C. (2010). Nanoparticles attenuate P-glycoprotein/MDR1 function in A549 human alveolar epithelial cells. *European Journal of Pharmaceutics and Biopharmaceutics*, *77*(3), 392–397.

Selvan, S. T., Yang Tan, T. T., Kee Yi, D., & Jana, N. R. (2010). Functional and multifunctional nanoparticles for bioimaging and biosensing. *Langmuir*, *26*(14), 11631–11641.

Shi, X., Li, D., Xie, J., Wang, S., Wu, Z., & Chen, H. (2012). Spectroscopic investigation of the interactions between gold nanoparticles and bovine serum albumin. *Chinese Science Bulletin*, *57*(10), 1109–1115.

Sperling, R. a, & Parak, W. J. (2010). Surface modification, functionalization and bioconjugation of colloidal inorganic nanoparticles. *Philosophical Transactions of the Royal Society*, *368*(1915), 1333–1383.

Sperlinger, R. A., Gil, P. R., Zhang, F., Zanella, M., & Parak, W. J. (2008). Biological applications of gold nanoparticles. *Chemical Society Reviews*, *37*(9), 1896–1908.

Strober, W. (2001). Trypan blue exclusion test of cell viability. *Current Protocols in Immunology*, *A-3B*.

Tiwari, P. M., Vig, K., Dennis, V. a., & Singh, S. R. (2011). Functionalized Gold Nanoparticles and Their Biomedical Applications. *Nanomaterials*, *1*(1), 31–63.

Tomaszewska, E., Soliwoda, K., Kadziola, K., Tkacz-Szczesna, B., Celichowski, G., Cichomski, M., … Grobelny, J. (2013). Detection limits of DLS and UV-Vis spectroscopy in characterization of polydisperse nanoparticles colloids. *Journal of Nanomaterials*, 1–10.

Turkevich, J., Stevenson, P. C., & Hillier, J. (1951). A study of the nucleation and growth processes in the synthesis of Colloidal Gold. *Discuss. Faraday Soc.*, *11*, 55–75.

Vasir, J., & Labhasetwar, V. (2008). Quantification of the Force of Nanoparticle-Cell Membrane Interactions and Its Influence on Intracellular Trafficking of Nanoparticles. *Bio*, *29*(31), 4244–4252.

Vercauteren, D., Vandenbroucke, R. E., Jones, A. T., Rejman, J., Demeester, J., De Smedt, S. C., Braeckmans, K. (2010). The use of inhibitors to study endocytic pathways of gene carriers: optimization and pitfalls. *Molecular Therapy*, *18*(3), 561–569.

Vigderman, L., & Zubarev, E. R. (2013). Therapeutic platforms based on gold nanoparticles and their covalent conjugates with drug molecules. *Advanced Drug Delivery Reviews*, *65*(5), 663–676.

Vinhas, R., Cordeiro, M., Carlos, F. F., Mendo, S., Fernandes, A. R., Figueiredo, S., & Baptista, P. V. (2015). Gold nanoparticle-based theranostics : disease diagnostics and treatment using a single nanomaterial. *Nanobiosensors in Disease Diagnosis*, *4*, 11–23.

Wilhelm, C., Gazeau, F., Roger, J., Pons, J. N., & Bacri, J. C. (2002). Interaction of anionic superparamagnetic nanoparticles with cells: Kinetic analyses of membrane adsorption and subsequent internalization. *Langmuir*, *18*(21), 8148–8155.

Xie, J., Lee, S., & Chen, X. (2010). Nanoparticle-based theranostic agents. *Advanced Drug Delivery Reviews*, *62*(11), 1064–1079.

Yang, L., Shang, L., & Nienhaus, G. U. (2013). Mechanistic aspects of fluorescent gold nanocluster internalization by live HeLa cells. *Nanoscale*, *5*(4), 1537–1543.

Yavuz, M. S., Cheng, Y., Chen, J., Cobley, C. M., Zhang, Q., Rycenga, M., Xia, Y. (2009). Gold nanocages covered by smart polymers for controlled release with near-infrared light. *Nature Materials*, *8*(12), 935–939.

You, J., Zhang, G., & Li, C. (2010). Exceptionally High Payload of Doxorubicin in Hollow Gold Nanospheres for Near-Infrared Light-Triggered Drug Release. *ACS Nano*, *4*(2), 1033–1041.

Zhang, Z., Wang, J., & Chen, C. (2013). Gold nanorods based platforms for light-mediated theranostics. *Theranostics*, *3*(3), 223–238.

Zhao, F., Zhao, Y., Liu, Y., Chang, X., Chen, C., & Zhao, Y. (2011). Cellular uptake, intracellular trafficking, and cytotoxicity of nanomaterials. *Small*, *7*(10), 1322–1337.

Zharov, V. P., Mercer, K. E., Galitovskaya, E. N., & Smeltzer, M. S. (2006). Photothermal nanotherapeutics and nanodiagnostics for selective killing of bacteria targeted with gold nanoparticles. *Biophysical Journal*, *90*(2), 619–627.

VI. APPENDIXES

A1. DETERMINATION OF THE DEGREE OF SATURATION OF GOLD NANOPARTCILES FUNCTIONALIZATION WITH PEG

To determine the quantity of PEG molecules to achieve a degree of saturation of 100%, a range of PEG concentrations were added to a fixed concentrations of citrate coated AuNPs (0 - 0.1 mg.mL^{-1}). The unbounded PEG was removed and the total thiolated groups present in the supernatants was quantified by the Ellmans's assay, using a calibration curve (Figure VI.1A). In this method, the thiol group of PEG chains present in the supernatant reacts with DTNB, giving a colored product that can be measured by UV-visible spectroscopy at 412 nm. The number of attached PEG chains were determined by the difference between the initial amount of PEG and the number of unbound chains calculated by the Ellmans's assay. The full degree of saturation was reached at 0.01 mg.mL^{-1} of PEG, since it was the last initial concentration where PEG molecules were not detected in the supernatant (Figure VI.1B). An increase of this initial concentration results on detection of PEG molecules in the supernatant, meaning that an excess of PEG was added in order to obtain 100% of saturation.

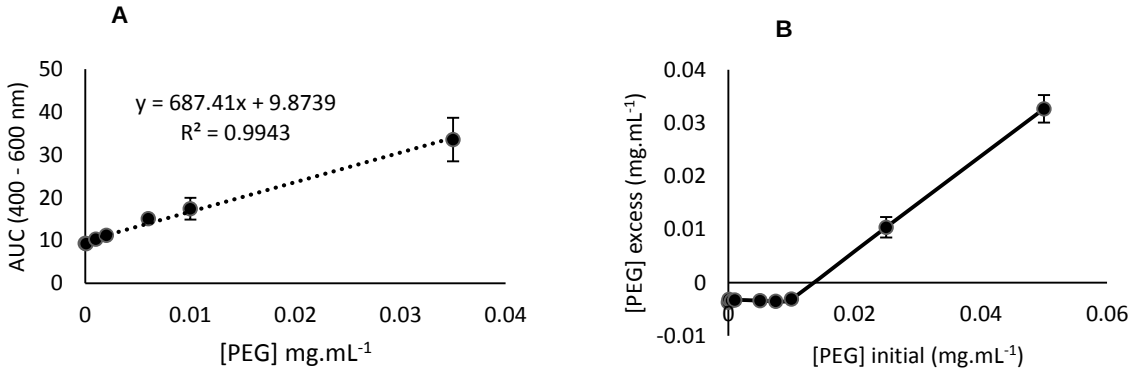

Figure VI.1 - (A) Standard calibration curve of PEG chains obtained by UV-visible spectroscopy. Data is relative to the average of three independent assays and error bars are correspondent to SEM. (B) Variation of the excess of PEG chains as function of initial concentration in the incubation with a fixed concentration of AuNPs (10 nM). At 0.01 mg.mL^{-1} of initial PEG concentration the 100% degree of saturation is achieved and for higher concentrations, PEG chains are detected in the supernatants. The data is relative to the average of three independent assays and error bars are correspondent to SD.

A2. QUANTIFICATION OF TAMRA MOLECULES PER AUNP BY FLUORESCENT MICROSOCOPY

To determine the amount of TAMRA attached to the AuNPs, a calibration curve was prepared in a range of 0 - 10^{-7} M of TAMRA in 2.5 mM MES buffer pH 5.9 under the same conditions of functionalization. The fluorescent intensity was quantified by fluorescent spectroscopy and plotted in function of TAMRA concentrations (Figure VI.2). After functionalization, the recovered supernatants were quantified by

fluorescent spectroscopy under the same conditions of the calibration curve, and the amount of TAMRA was quantified by interpolation of the calibration curve.

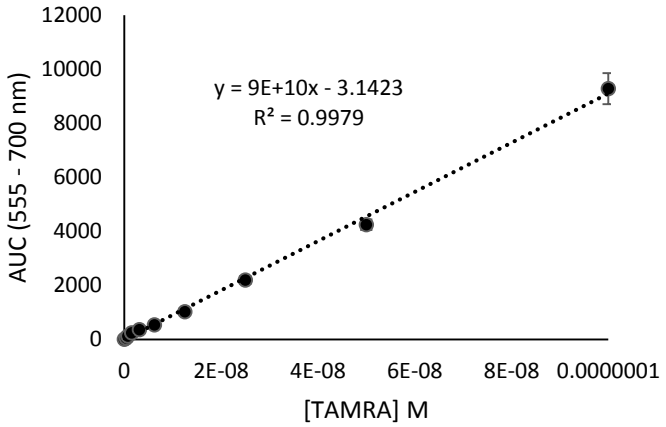

Figure VI.2 - Standard calibration curve of TAMRA concentration obtained by fluorescent spectroscopy. The data is relative to the average of three independent assays and error bars are correspondent to SD.

All the measurements were taken in a Cary Eclipse Fluorescence spectrophotometer at excitation wavelength of 493 nm and recorded in a frequency range of 500 - 700 nm, at 600 nm/min with a photomultiplier potency of 600 V, using quartz cells with 1 cm of excitation path (105.254-QS, Hellma, Germany).